Section on Functional Imaging Methods
(2015-2020)

Peter A. Bandettini, Ph.D., Chief
Report for Board of Scientific Counselors' Review

Table of Contents

Executive Summary

It has been almost thirty years since functional MRI (fMRI) was first demonstrated, and during this time, it has been embraced as an essential tool for a wide range of neuroscience and clinical questions. This widespread utilization has been driven by fundamental advances in fMRI methodology that continue to improve its precision, reliability, and interpretability. Functional MRI methodology includes MRI hardware; pulse sequences for high temporal and spatial resolution as well as hemodynamic specificity; image reconstruction; artifact and large vessel identification and mitigation; hemodynamic transfer function characterization; multi-modal integration; paradigm design; time series analysis; group and subject comparison; and computational and network model integration.

MRI pulse sequences include strategies for higher temporal and/or spatial resolution acquisition as well as increased brain coverage. They are also designed for selective hemodynamic contrast sensitivity. In recent years, contrast sensitivities have included gradient-echo blood oxygen level dependent (BOLD) contrast – sensitive to all vessel sizes, spin-echo BOLD – sensitive to both small compartments and small vessels, arterial spin labelling (ASL) - sensitive to perfusion, vascular space occupancy (VASO) – sensitive to blood volume changes, and multi-echo EPI (ME-EPI) which has the ability to tease out pure BOLD effects from inflow and motion. SFIM has been developing, testing, and applying these novel pulse sequences as indicated in the report.

Time series analysis is intertwined with paradigm design strategies. Over the years, paradigm designs have evolved to include event-related, hybrid blocked/event-related, neuronal adaptation, resting state, naturalistic stimuli and/or free behavior tasks, and real time feedback. Likewise, analyses have evolved to include correlation or connectivity analysis, dynamic connectivity analysis, multivariate decoding and encoding, and inter-subject correlation (ISC). Features beyond just fMRI magnitude and correlation have included undershoots, transients, latencies, and shapes. For multivariate decoding, voxel-wise activity patterns have been found to be informative. Model free approaches including Independent Component Analysis (ICA) and ISC, as well as deep learning approaches, have proven to be useful for both exploratory and hypothesis-driven analysis. Analysis methods tailored to multi-echo acquisition have been developed to identify and keep those components which show BOLD contrast as revealed by an echo time (TE) dependence in the data. SFIM has been developing, testing, and applying many of these paradigm and processing approaches, as indicated in the report.

Over the past twenty years, the Section on Functional Imaging Methods (SFIM) has been working on the advancement, refinement, and application of every methodology mentioned above. SFIM is focused on increasing the utility of fMRI to catalyze new clinical and basic research insights and applications. The expertise of our group is diverse, including MR physicists, engineers, computer scientists, basic neuroscientists, and cognitive neuroscientists. We collaborate with other groups in NIMH and around the world that apply our methods to study specific neuroscience questions in healthy volunteers and patient populations.

Over the past four years, SFIM's two primary areas of focus have been **ultra-high spatial resolution fMRI at high field (7 Tesla)** and **understanding and leveraging time series information.** For our high-resolution focus, we have developed pulse sequences, paradigms, and processing pipelines to probe layer and column specific activation across the entire brain. For our time series focused studies, we have developed novel methods for decoding and mapping brain activity and for characterizing differences and similarities between individuals using naturalistic paradigms combined with ISC assessment or within-subject dynamic connectivity-based measures. We are developing MRI data driven methods to characterize ongoing vigilance fluctuations, and we have developed methods for rapidly decoding brain activity using event-related paradigms. In our rapid decoding study, we found that use of multivariate patterns appears to naturally bypass problematic hemodynamic variability as large vessel responses contain less informative decoding information.

Significance

A wealth of both neuronal and physiologic information remains untapped within the fMRI spatial-temporal signal patterns. Advancements in methodology for extracting and parsing this information require not only better tools but a deeper understanding of the basis of the signal and the noise. Our group focuses on both improving the tools and increasing the understanding of the fMRI signal, opening up the utility of fMRI for addressing increasingly nuanced and penetrating questions in neuroscience.

A complete understanding of the brain will be that which integrates data and generates principles that span all salient temporal and spatial scales of organization. High resolution fMRI, having sub-millimeter voxel dimensions, promises to link our understanding of whole brain systems level with circuit level scales. It has also ushered in a new spatial dimension - that of cortical layers - for mapping and understanding human brain function. Insight into layer-specific activity promises to shed light on cortical hierarchy, connectivity, and computation.

Recent years have seen progress in computational models that simulate macroscale features of brain dynamics using networks of interconnected regions. These models typically include a structural backbone consisting of anatomical tract data from diffusion tensor imaging (DTI) and functional data from electroencephalography (EEG) and/or fMRI. EEG has high temporal resolution; however, it mostly reflects activity in excitatory superficial layer neurons closest to the skull and oriented perpendicular to the scalp, giving an incomplete picture of cortical dynamics. Data from layer fMRI can help fill this gap. Approaches to infer cascading activation and thus connection directionality have been made using fMRI[1,2]; however, these are problematic as intrinsic hemodynamic latencies vary quasi-randomly up to 4 sec across voxels. Layer fMRI may provide information to help infer feedforward and feedback directionality directly from known laminar-specific patterns of activity.

Regarding our work on time series analysis, deriving meaningful information and mitigating noise involves iteration between what we know with what we don't know. We use our knowledge of brain activity, the hemodynamic signal, and the noise so that neuronal information may be extracted without making too many or too rigid assumptions that miss salient information. In most of our studies in this section, our paradigm designs and analyses make use of what we know from external measures, brain activity timing, the hemodynamic response, and the noise to obtain novel information. We use correlation dynamics over time, activation corresponding to those correlation dynamics, as well as inter-subject correlations with identical naturalistic paradigms to derive information about the subjects' traits, states, or brain activity. We also use external measures of traits, task performance, or arousal to constrain and add meaning to the information that we obtain using fMRI. Our goal is the full separation of noise from meaningful neuronal signal. This goal is fundamentally important as it would increase the utility of fMRI towards better informing models of brain organization, "reading out" of ongoing cognition, and catalyzing the creation and dissemination of neuromarkers of either normal or pathological states, traits, and conditions. These improvements, coupled with more efficient and practical clinical pipelines, are also fundamental for fMRI to be more fully embraced as a clinical tool.

Innovation and Appropriateness to the Intramural Environment

In the past four years, our group has innovated in two general directions. The first is the development of novel high functional resolution pulse sequence and processing approaches for identifying hemodynamic changes most localized to neuronal activity, allowing for high resolution fMRI maps of layer activity and connectivity. The second is the design of paradigms and time series processing approaches to capture ongoing thought processes and activation during rest and naturalistic stimuli, and to allow delineation of differences in subject traits based on neuroimaging data. A working principle that we have used is that information is optimally derived when time series models are neither too constrained nor too open-ended. We aim to iterate at the limits of what we know about the behavior of the subjects and their corresponding neuronal activity and hemodynamics, striving to assist our interpretation through what we know about pulse sequence sensitivities, paradigms, known activation patterns, and behavioral measures.

We developed novel pulse sequences that lend themselves to rapid high-resolution functional imaging at high field. We developed novel paradigms and processing approaches for deriving cortical feedforward and feedback information as well as hierarchal cortical organization using layer specific activation and resting state connectivity. From these methods, we discovered a unique digit organizational structure based on two different finger movement patterns. We demonstrated the ability to derive measures of ongoing cognition from resting state data. We used dynamic connectivity as well as a novel inter-subject connectivity approach to derive trait and performance information. We have also demonstrated that not only is task decoding possible using event-related fMRI but that the use of decoding measures rather than the hemodynamic response itself naturally bypasses the limits of more delayed draining vein effects thus increasing the temporal accuracy of fMRI.

The research performed in the past four years in SFIM is appropriate to the intramural environment because it requires the high field systems, the considerable physical resources, and the extensive data analysis expertise that extends beyond our immediate group. Collaboration with fellow IRP PIs, Cores and Teams has been critical to the success of these projects. Collaboration with other groups that focus on patient populations and specific neuroscience questions has been essential for the testing and refinement of our methods.

Lastly, and importantly, the stable funding structure of the NIMH Intramural Program allows our group to focus on the long-term goals of method development without the requirement of obtaining funds to address a specific biological hypothesis, with method development as a secondary goal. Rather, our work naturally iterates between long term method development and collaboration with investigators who may most benefit from the methodology we produce. This stable environment fosters long term method advancement which, in the extramural environment, may be stifled as extramural funding is relatively short term and focused on questions that are separate from the methods themselves. Again, we feel that method advancements have fundamentally driven the utility of fMRI over the past thirty years and the stable intramural environment for fostering method advancement is not only ideally suited for our goals, but deeply and uniquely beneficial to the success of fMRI as a field.

Background and Progress

High Spatial Resolution fMRI

Layer fMRI began with studies of primary motor and visual systems and is currently beginning to be used to explore the interplay of feedforward and feedback activity across the entire brain[3]. Layer fMRI is challenging, as mitigation of subject motion and large vessel artifacts is critical for interpretable data. Over the past four years, SFIM has been developing high resolution and small vessel-specific fMRI pulse sequences[4,5], layer segmentation and processing pipelines[6], and unique analytic approaches to more cleanly map and interpret the detailed functional information available[7].

Here, we report on our high-resolution fMRI work in two parts: completed work and ongoing work. For our completed work, we first compare the functional sensitivities and vascular specificities of different pulse sequence contrasts. In most of the studies mentioned, we use simultaneously collected BOLD and VASO contrast which allows both BOLD vs VASO comparisons as well as complete removal of all BOLD effects from the cerebral blood volume estimates through pairwise image division. In our next study, we demonstrate modulation of layer activity in M1 with different motor tasks and tactile stimuli. In a second motor cortex study, we reveal a novel digit representation in M1 that shows sensitivity to the type of movement performed. We then demonstrate that activity in upper and lower layers of the somatosensory cortex (S1) are sensitive to sensory prediction while the middle layer of S1 is activated by sensory input. We go on to show that, during working memory and manipulation tasks, upper layers of the Dorsal Lateral Prefrontal Cortex (DLPFC) are selectively activated, while lower layer activity is only associated with the subsequent motor response. Lastly, we conclude this section with our work exploring resting state connectivity across layers, revealing the hierarchal structure of the visual system by characterizing the layer connectivity profile across the entire cortical ribbon with a seed region that is systematically shifted along the cortical ribbon. Furthermore, we apply cortical column resting state "hub mapping" to characterize layer resting state power profiles across the brain, revealing a striking differentiation between frontal and parietal regions.

In ongoing work, we demonstrate a unique calibration approach that maps the ratio of simultaneous VASO and BOLD contrast to reveal voxels containing large vessels. Secondly, we report on our ongoing work using our novel integrated VASO and PERfusion (VAPER) pulse sequence to probe layer activity associated with visual-auditory functional activation in the planum temporale. Lastly, we report on a novel whole brain VASO sequence and demonstrate preliminary approaches for exploring this explosion of data as we add a layer dimension to a whole brain connectome data set.

Completed work

Sensitivity vs. Specificity

A major challenge for inferring layer-dependent activity has been to use the fMRI contrast that has the best combination of specificity to microvascular responses that are proximal to neuronal activity and enough sensitivity to detect activity changes within a practical limit of an hour of averaging. Here we compare pulse sequences using contrast mechanisms sensitive to different aspects of the hemodynamic response, including VASO [8], SE-BOLD (Spin-echo BOLD – a combination of T2 and T2* weighting), T2/T1ρ-prep-BOLD ("pure" T2 weighting), and diffusion weighted T2-prep-BOLD ("pure" T2 with intravascular BOLD removed)[7]. Experiments were performed on a 7T Siemens scanner with a 32-channel Nova head-coil. Four volunteers participated in 18 experiments. All experiments were conducted with 0.7 mm x 0.7 mm in-plane resolution with 1.5 mm thick slices that were aligned to be perpendicular to the cortical surface of M1. All scans used GRAPPA 2 acceleration.

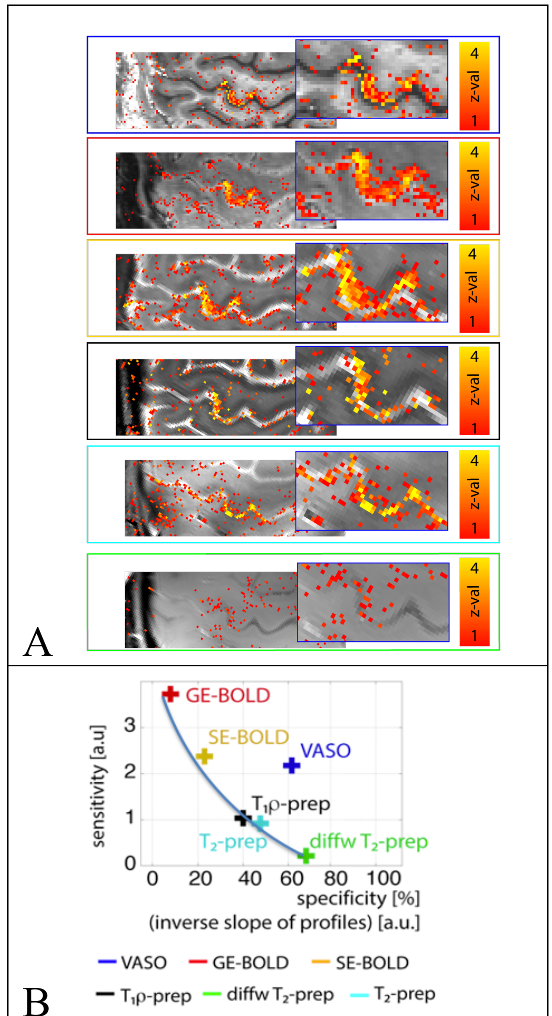

Figure 1: Comparison of functional contrasts: A) Maps of motor cortex activation and B) Corresponding plot of sensitivity (as determined by statistical significance of the signal changes) vs. specificity (as determined by the sharpness of the M1 layer activation profile) shows that VASO is a promising compromise.

Figure 1 shows motor cortex activation images superimposed on the corresponding structural images for each sequence. It also compares the contrasts in terms of sensitivity and specificity[9]. VASO is among the most specific contrast, yet it also has sufficient sensitivity for layer-fMRI. We attribute this to blood volume sensitivity that includes small feeding arteries that are localized to the region of activation. While VASO clearly is advantageous in terms of contrast, its most common manifestation has limited coverage and low time efficiency because of the need for an inversion pulse to null the blood signal. Versions of VASO have recently been developed that do not rely on the long blood nulling waiting time, and therefore can be used in whole brain functional imaging. *{Within SFIM: Laurentius Huber, Yuhui Chai, Emily Finn. Outside of SFIM: Sean Marrett, Jun Hua, David Feinberg, Harald Moeller, Kamil Uludag, Valentin Kemper}*

Selective Layer Activation in Motor Cortex

Our study demonstrating layer modulation in primary motor cortex (M1) was published since our last BSC report[9]. We used simultaneously acquired 0.75 mm x 0.75 mm x 1.5 mm voxel dimension VASO and BOLD contrast time series covering a slab containing M1 in 11 participants. Across separate time series, subjects performed a contralateral tapping task, contralateral movement without tapping, contralateral sensory stimulation, and an ipsilateral finger tapping task. These tasks were designed to modulate the level of activity of upper (cortical input from sensory cortex), and lower (output to spinal cord) layers. Our results, shown in Figure 2, demonstrate the predicted modulation in upper and lower cortical layers with the different tasks. It can be seen in the layer profiles shown that VASO-based blood volume changes more clearly differentiate layer modulation than BOLD contrast does. Finger movement with tapping activates both upper and lower layers. Movement without touching the fingers dampens both input and output. External touching of fingers activates only the upper (input) layers. Ipsilateral finger movement with touching appears to inhibit upper layer activity while contributing to no change in lower (output) layers. *{Within SFIM: Laurentius Huber, David Jangraw, Daniel Handwerker, Harry Hall. Outside of SFIM: Sean Marrett, Gang Chen}*

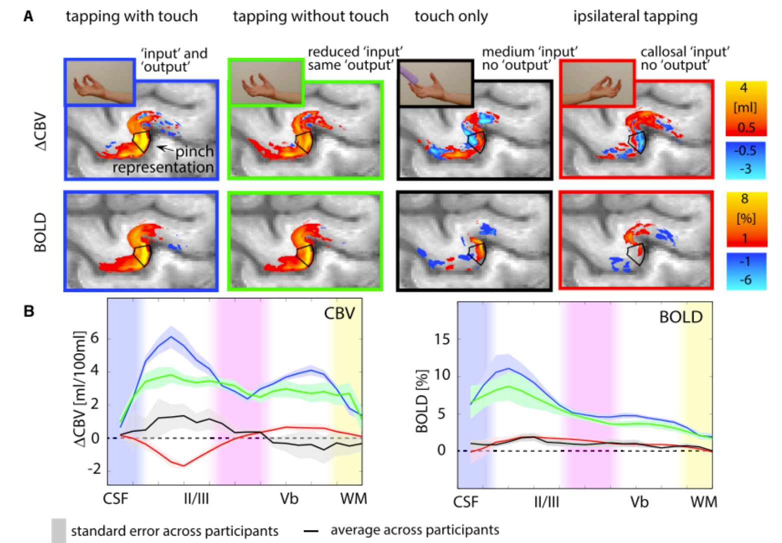

Figure 2: Averaged layer-dependent fMRI responses in M1 of all participants in response to four different sensorimotor tasks. A) The four tasks evoked fMRI signals that varied with cortical depth in the thumb-index finger pinch motor area, indicated by the black box. B) The average cortical profiles across all participants from the boxed ROI in the maps show different laminar patterns in superficial and deep cortical laminae for the different tasks. Shaded areas around the plots are the standard error across participants. BOLD contrast shows the expected weighting towards superficial layers due to draining pial vessels.

Functional Mapping of Sensorimotor Digit Organization

Our high-resolution studies in motor cortex have not been limited to layer-specific mapping. The increased specificity of blood volume-based VASO contrast allows finer differentiation of individual digit representations in sensory and motor cortex[10]. In this study, five participants underwent 84 hours of scanning at 7T using VASO contrast at 0.8 mm x 0.8 mm x 1 mm voxel dimension. Subjects performed two classes of tasks. First, they performed an individual digit tapping task, and, in a follow-up, alternated between a full hand grasping task and a retraction task – both against resistance. Figure 3 shows the imaging plane localization and the results. We found, in all participants' M1, two separate digit representations arranged in a mirror image manner to each other. We found only a single digit pattern in S1. For the grasping vs retraction tasks, we found preferential activation for grasping in only one of the digit patterns in M1 and in the entire S1 region previously mapped out in the digit task. For the retraction task, we found preferential activation in the immediately adjacent mirror imaged pattern in M1 yet minimal activation in S1. This organizational structure was present in all five participants. Figure 4 shows the results from all five participants, demonstrating reproducibility. We believe these findings are novel in that they suggest that the digit representation is dependent on the type of action performed. This finding is supported by recent reports of unique patterns of activation corresponding to complex hand postural position[11]. *{Within SFIM: Laurentius Huber, Emily Finn. Daniel Handwerker. Outside of SFIM: Sean Marrett, Daniel Glenn}*

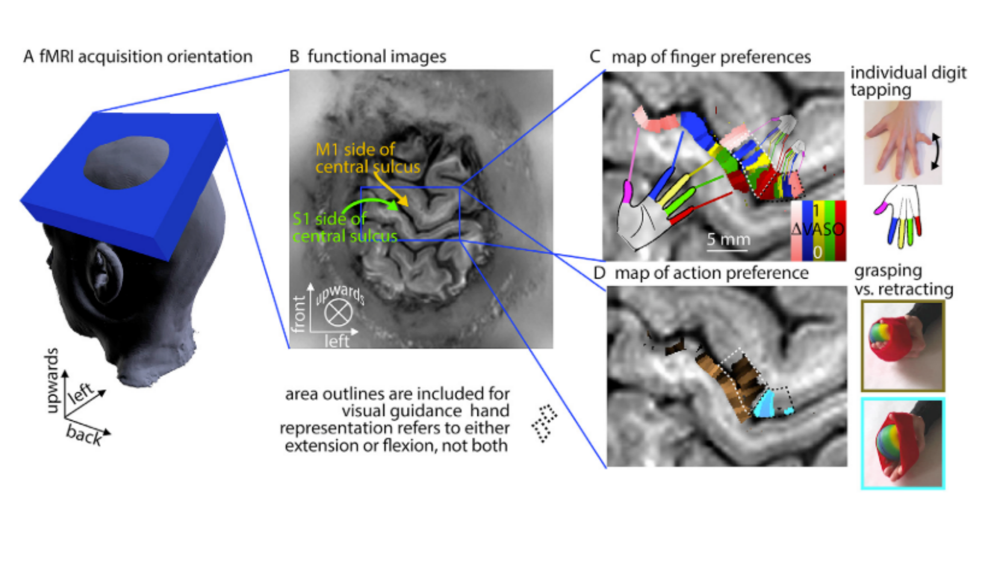

Figure 3: Acquisition and analysis methods for measuring the laminar and columnar functional topography. A-B) The imaging slab is aligned to cover the entire primary sensorimotor cortex. C) The functional CBV signal changes obtained using a five-finger left hand tapping task reveal individual digit representations in M1 and S1. While S1 has a homunculus like linear representation of individual digits, the primary motor cortex shows clear deviations of the homunculus model. D) While S1 has a stronger activity for grasping compared to retraction motor actions, the primary motor cortex shows individual patches of areas that are either specific to grasping or retraction actions.

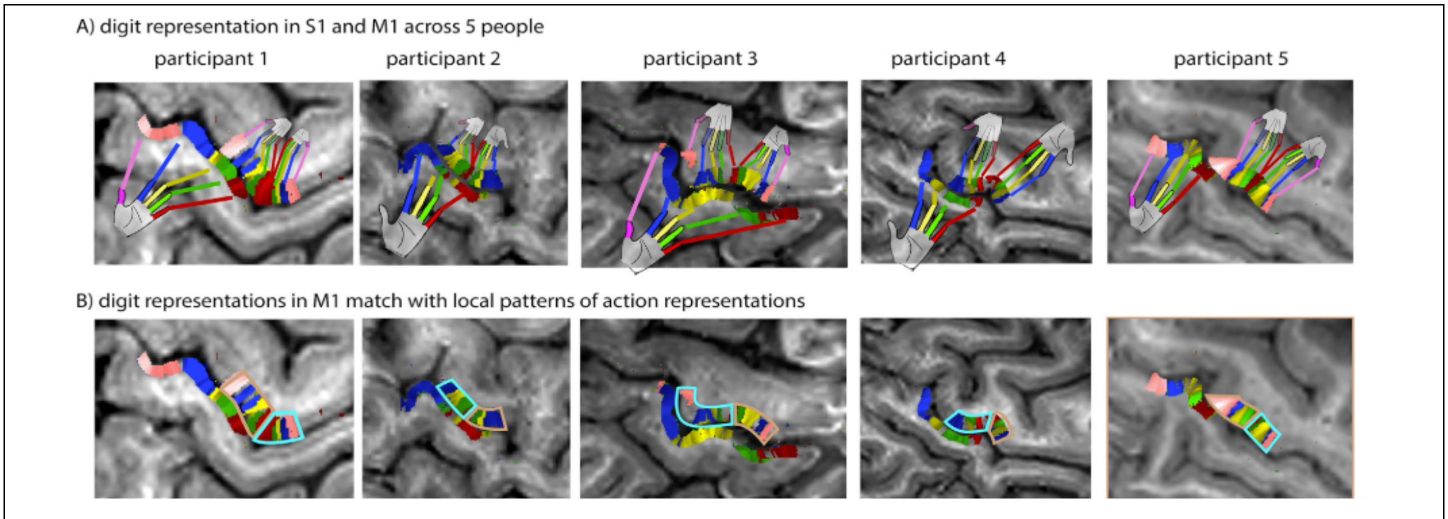

Figure 4: Multiple hand representations across participants. A) The finger dominance maps show that S1 has a single representation of each finger in all participants, while M1 has multiple finger representations for each finger. The representations of the digits in M1 are mirrored and about half the size of the representations in S1. B) The spatial pattern of multiple finger representations in M1 is compared to the representations of grasping and retraction of a ball, shown, respectively, as the copper and turquoise outlines Each set of fingers is clearly outlined by the borders of the regions showing grasping or retracting preference.

Digit-Specific Layer Modulation with Tactile Prediction

When humans perceive a sensation, input from sensory receptors is received in layer 4 of S1 and processed based on expectations that presumably project to upper and lower layers of S1[12]. The precise mechanisms of this predictive coding in the human somatosensory system are not fully understood. In this study, we aimed to map the cortical layers involved with predictive processing of somato-sensation by examining the layer-specific activity in sensory input and predictive feedback in S1, and specifically in area 3b. We acquired submillimeter fMRI data at 7T in ten subjects during either predictable or unpredictable finger stroking sequence. We demonstrate that the sensory input from thalamus preferentially activates the middle layer in area 3b while the superficial and deep layers are more engaged for cortico-cortical predictive feedback input.

Figure 5 shows the experiment and results. In figure 5A, the functional locations of digit stimulation (D1-4) are shown along the postcentral gyrus. A model for the thalamus input and cortical input are shown at the bottom. Figure 5B illustrates the input to layer IV from the thalamus to each digit region in area 3b. Layer activation profiles from D1 through D4 are shown, highlighting activation in layer IV and only present during the stroking of the corresponding digit (D1 and D3 shown here). Figure 5C shows activation maps (and zoomed maps of D1 activation) clearly depicting activation across all layers in area D1 corresponding to stroking all four fingers in a predictable order. When stroking all four fingers in a random order, only activation in middle layers appears. Upper and lower layers, corresponding to predictive cortical input, are not activated as the random sequence does not allow the formation of a clear prediction model. When stroking fingers yet leaving out D1, predicted activity is only shown as activity in superficial layers yet no activity is seen in layer IV of D1. Lastly, when the stroking sequences is random and leaves out D1, there is no activation seen in D1 at all.

This study demonstrates functional differentiation of layer activity in approximate agreement with the current understanding of layer processing. As layer IV receives sensory input via the thalamus, it is active during stroking. The upper and lower layers are presumably activated by expectation of finger stroking and diminishes when the sequence of stroking is random. *{Within SFIM: Yinghua Yu, Jiajia Yang, Laurentius Huber, David Jangraw, Daniel Handwerker, Peter Molfese. Outside of SFIM: Gang Chen}*

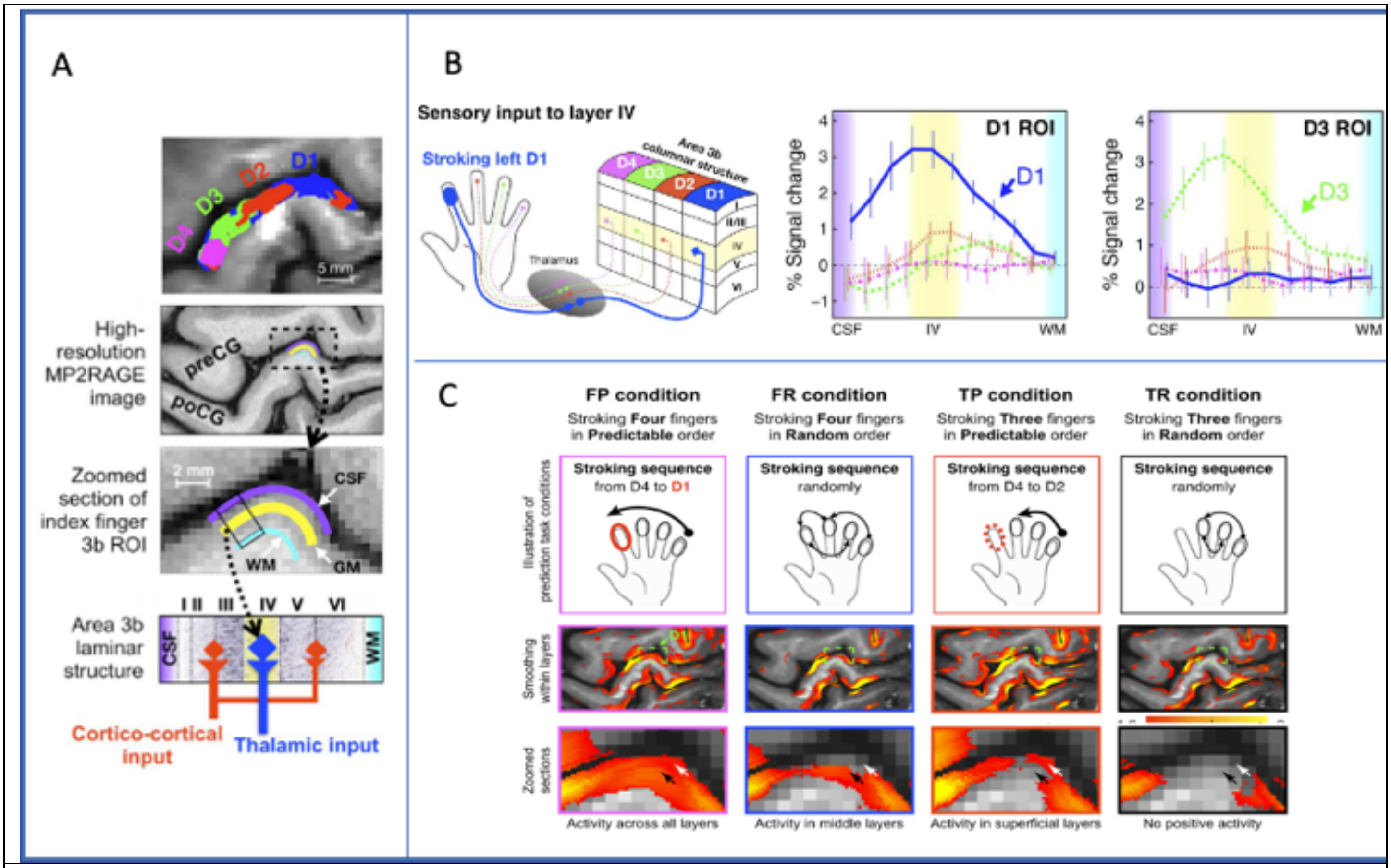

Figure 5: Modulation of sensory input and expectation. A) Functional location of digits (4 through 1) and inputs to layers in each digit. B) Sensory input to layer 4, and corresponding layer profiles with each profile corresponding to a different digit being stroked. In D1 ROI, stroking causes selective activation of layer 4, and likewise for the D3 region. C) The four conditions and the corresponding maps of activation in the region corresponding to D1 activation. Predictable order including D1 stroking activated all layers. Non-predictable order diminished activation in upper and lower layers, yet preserved the middle layer activation. Predictable stroking, leaving out D1, caused diminished activation in layer IV, yet activated superficial layers. Lastly unpredictable stroking, leaving out D1, did not activate the functional region corresponding to D1 at all.

Layer-Specific Activation in Dorsal Lateral Prefrontal Cortex

We have developed and extended high-resolution fMRI methods for use in high-order cognitive brain regions and used these methods to show cortical-depth-dependent patterns of activity in DLPFC during different periods of a working memory task[13]. This work is the first to detect layer-specific signatures of activity in the association cortex. We achieved this result thanks to several innovations, including: 1) extending a cerebral-blood-volume-based contrast mechanism, VASO, for use in areas of the association cortex where folding patterns are less predictable and anatomy is less consistent across participants; 2) using an online functional localizer to optimize imaging volume placement in each participant; 3) using a task design that allowed for separation of signal between different periods within a trial (e.g., encoding, delay, response) even in the face of a relatively low temporal resolution, which was necessary to achieve the desired high spatial resolution to separate cortical layers. Applying these methods to data acquired at 7T from 15 participants scanned during a working memory task, we detected layer-specific activity time series in the DLPFC that follow the hypothesized patterns: namely, superficial layers were preferentially active during the delay period, specifically in trials requiring manipulation (rather than mere maintenance) of information held in working memory, and deeper layers were preferentially active during the motor response. Figure 6 shows that effects were visible in individual subjects. While VASO contrast shows more clear delineation of activity, BOLD contrast was also able to differentiate upper and lower layer activity with the maintenance and motor task respectively. This study opens the door to mapping information flow during cognitive process in awake, behaving humans. *{Within SFIM: Emily Finn, Laurentius Huber, David Jangraw, Peter Molfese}*

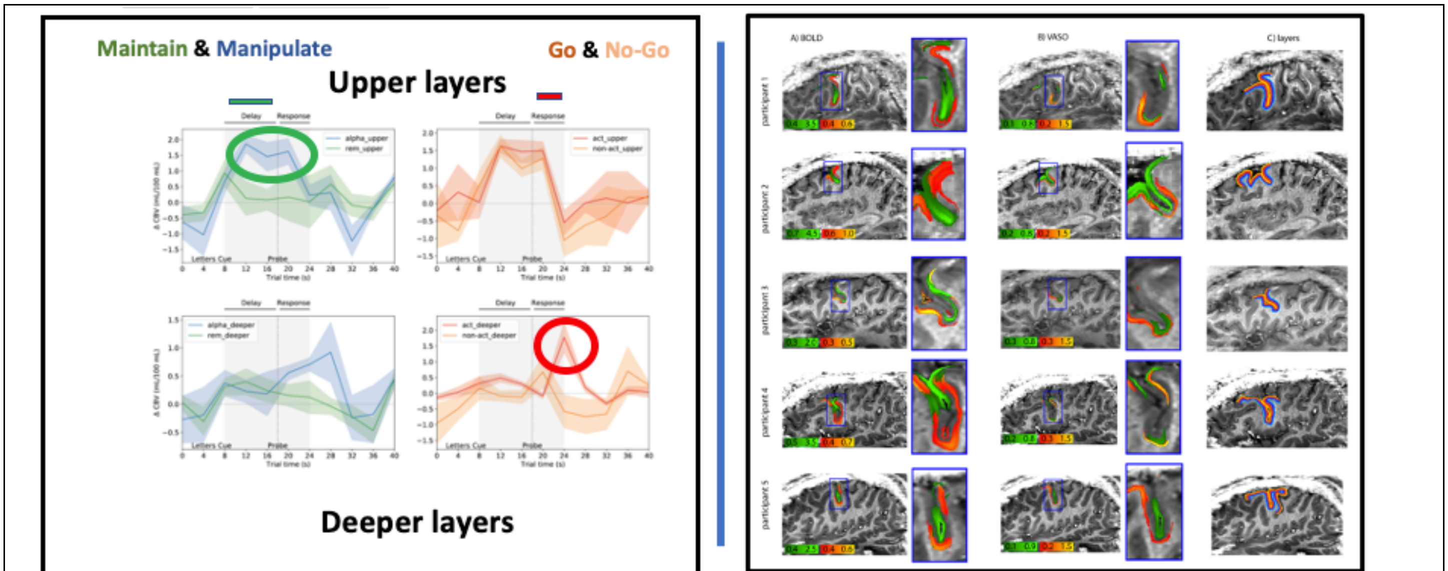

Figure 6: Selective activation in the upper layers in DLPFC *during* a memory or manipulation task and in lower layers during the response *at the end of* the maintain or manipulate time period. Note that no activation is seen if no motor action is performed. Activation maps show upper layer activation in green and lower layer activation in red for both BOLD and VASO contrast, however VASO delineates the activation more precisely.

Resting State Assessment of Visual Hierarchy

In a canonical cortical microcircuit, feedforward activity is in middle cortical layers, while feedback activity is in superficial and deeper layers[14]. To the degree that this canonical relationship applies, it may be possible to classify whether a given cortical area is best described as predominantly feedforward or feedback driven based on the connectivity or resting state activity profile across layers of this area[7]. Here we developed an approach to classify columnar sets across the cortex based on comparing the profile of resting state connectivity across the cortical layer to two templates representing feedback vs. feedforward driven activity as shown respectively by the blue and red curves in Figure 7A. The time courses of manually selected seed regions were used as regressors. Correlation values with the regressor were calculated along the cortical profile, across layers, for every columnar structure. The term "columnar structure" is not strictly a cortical column here, but rather a small segment of cortex extending through all layers. For this analysis, we segment the entire cortical ribbon into these "columnar structures." The calculated correlation value layer profiles for each columnar structure were compared with the feedforward vs feedback templates to classify columns as having feed-forward or feedback dominance relative to the seed region. This procedure was repeated for 8 manually selected seed regions along the visual processing stream. The resulting feed-forward (blue) vs. feedback (red) driven maps of this seed-based classification algorithm were used to determine which areas receive feedforward input from the seed and which areas receive feedback input from the seed. As is shown in Figure 7, when the seed region is in the thalamus, the correlation profile along the entire cortical ribbon is classified as receiving feedforward input (blue curve and blue map). As the seed region is moved along the cortical ribbon, visual areas lower in the cortical hierarchy than the seed region change their connectivity profiles to reflect feedback dominated activity (red curve and red map).

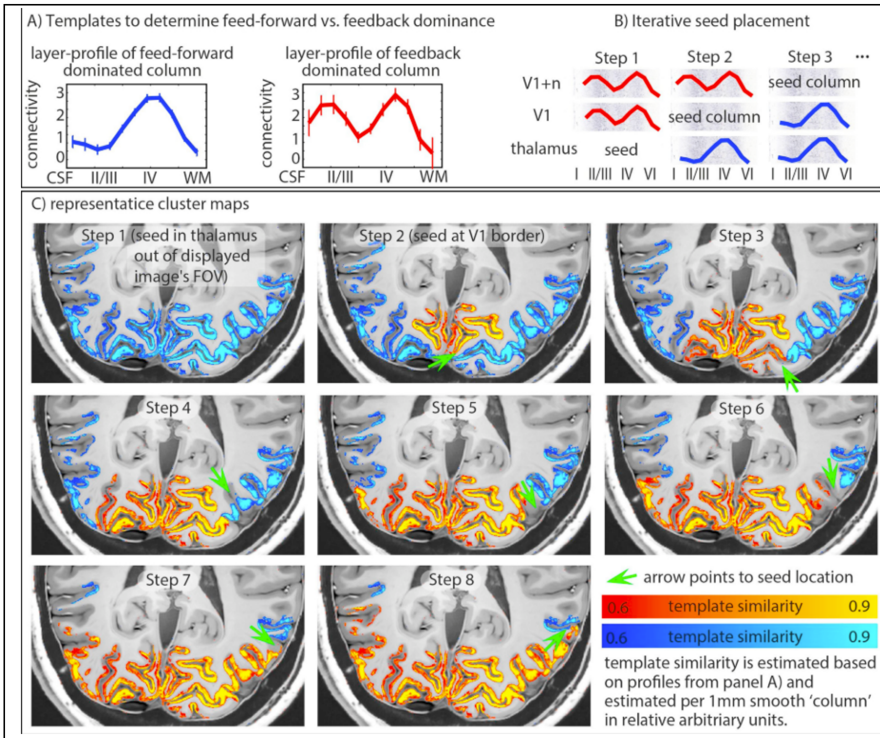

Figure 7: Hierarchy mapping procedure by means of a seed-based layer-dependent analysis. A) First, characteristic layer-dependent profiles are determined. At 0.8 mm resolution, feedback activity in superficial layers (II/III) and deeper layers (IV/VI) can be separated as two separate peaks (red). Feed-forward activity in the deep layer IV can be seen as a single peak in the middle/deeper cortical depth (blue). B) For a given seed region, the layer-profile is determined for all columns. Here 'columns' are considered as smooth 1mm patches of the cortex. Each column's layer-profile can then be clustered into one of the predefined classes based on the highest relative correlation strength. Columns with layer-profiles that are dominated by superficial and deeper layer activity are considered to mostly receive feedback input from the seed region. Columns with layer-profiles that are show predominantly middle layer activity are considered to mostly receive feed-forward input. C) Example clusters for seed regions indicated with green arrows. Clusters of feed-forward and feedback dominance are bilaterally organized along the geodesic distance.

We have modified the above approach in order to classify the seed-independent *predominant* activity (either feedforward or feedback) across all connections in each columnar set in the brain by comparing fluctuation dominance across the cortical depth profiles. For this seed-independent approach, we estimated the "hubness" of every layer within every columnar unit, as shown in Figure 8. We calculated the correlation of the time series of each individual layer in a column with all other layers in that column. When the correlation of any given layer time series with all other layers is high, this suggests that this layer best represents predominant fluctuation power in the entire columnar unit. When the correlation of any given layer is low, it suggests that this layer is not contributing significantly to the overall ongoing fluctuations in that columnar unit. The resulting feed-forward vs. feedback driven map of this ROI independent classification, using the templates in Figure 8C, can be used to indicate which areas have resting-state fluctuation that are pre-dominantly associated with feedforward or feedback activity. Using this approach, we observe a striking delineation between frontal and parietal areas of the brain. Frontal areas appear to show predominantly feedback activity, while parietal areas appear to show predominantly feedforward activity. It is premature at this point to speculate on the functional significance of this differentiation. *{Within SFIM: Laurentius Huber, Emily Finn, Yuhui Chai. Outside of SFIM: Rainer Goebel, Rudiger Stirnberg, Tony Stocker, Sean Marrett, Seong-Gi Kim, SoHyun Han, Benedikt Poser}*

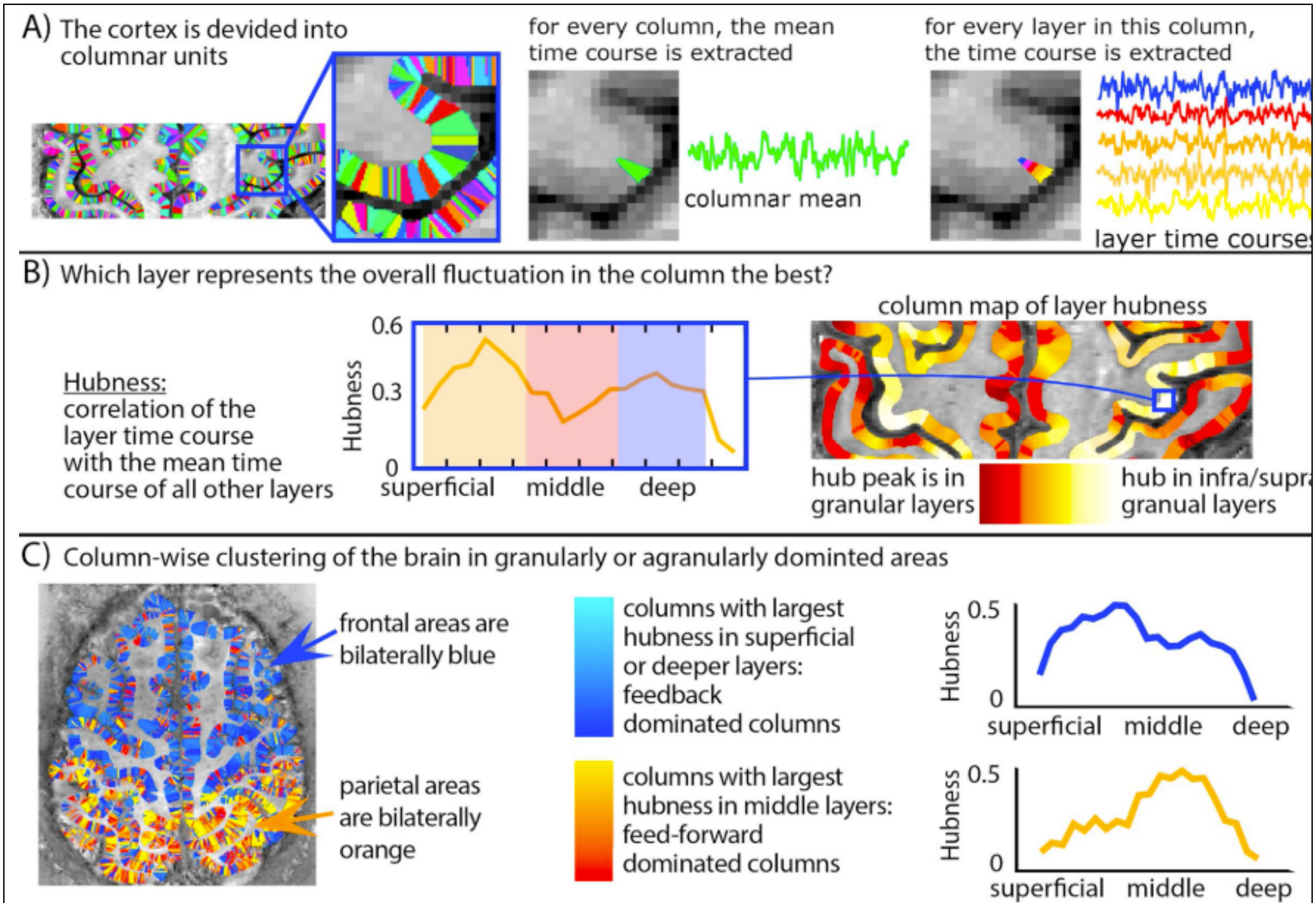

Figure 8: Mapping the columnar-specific layer "hubness" across brain areas. Calculating the hubness of every layer in a column allows the generation of hubness layer- profiles. A) The cortex is parceled into columnar structures. The resting-state time course of every columnar unit is extracted. B) The layer-specific fMRI fluctuations are used to determine a functional measure of hubness. The term 'hub' is used here to describe nodes (e.g. layers) with exceptionally higher functional connectivity compared to other nodes. These nodes are thought to play a major role in the coordination of information flow within brain networks. Here, hubness is defined as the correlation between the layer-specific time course and the mean time course of all remaining layers within each column. C) This is an example of clustering the brain into feed-forward driven areas with largest hubness measures in the granular layer versus feedback driven areas with largest hubness measures in infra-granular and supra-granular layers. A sharp division between frontal (feedforward) and parietal (feedback) areas at the central sulcus can be seen.

Ongoing Work

Vascular calibration

From Figure 1, it's clear that gradient-echo (GE) BOLD contrast shows the highest sensitivity yet the lowest layer specificity. If GE-BOLD were to be calibrated to improve specificity, it would be preferred because, in addition to having the highest sensitivity, it allows acquisition of whole-brain data with a relatively short TR. Here, we show a promising calibration approach that may prove useful not only for standard resolution BOLD studies – allowing more quantitative and precise use of the BOLD signal, but also for layer fMRI. In a previous study, we demonstrated the validity of a method called VasA[15] that is based on the observation that global slow respiration-induced BOLD changes can be used as an indicator for cerebral vascular reactivity and baseline venous CBV, allowing voxel-wise calibration. In a follow-up study, shown in Figure 9, we characterized the voxel-wise relationship between simultaneously obtained VASO and BOLD contrast time series. Here, we measured the ratio between the BOLD and VASO signal changes and found a distinct pattern that the higher the ratio between BOLD and VASO changes, the more clearly these signals were in draining veins in the sulci, and likewise, as the ratio decreased, approaching 1, the changes were predominantly in gray matter. To investigate this further, we performed independent component analysis on the BOLD time series from simultaneously acquired BOLD and VASO data sets that were collected during motor cortex activation. ICA components that clearly mapped to veins showed a high ratio, while those that showed layer specific responses, confined to grey matter, showed a ratio approaching 1. This analysis approach has promise in leveraging both the higher sensitivity of BOLD and the higher specificity of VASO to eliminate large vessel effects in low resolution BOLD studies but to allow the use of BOLD for assessment of layer specific activation. While ICA analysis of BOLD differentiates these regions of activation, it is only by assessing the ratio between BOLD and VASO, that the microvascular source of the BOLD signal can be confirmed. We plan to follow up on this in future studies to determine the efficacy of using this calibration factor in layer BOLD fMRI to eliminate across-layer vascular effects. *{Within SFIM: Laurentius Huber. Outside of SFIM: Samira Kazan, Guillaume Flandin, Dimo Ivanov, and Nikolaus Weiskopf}*

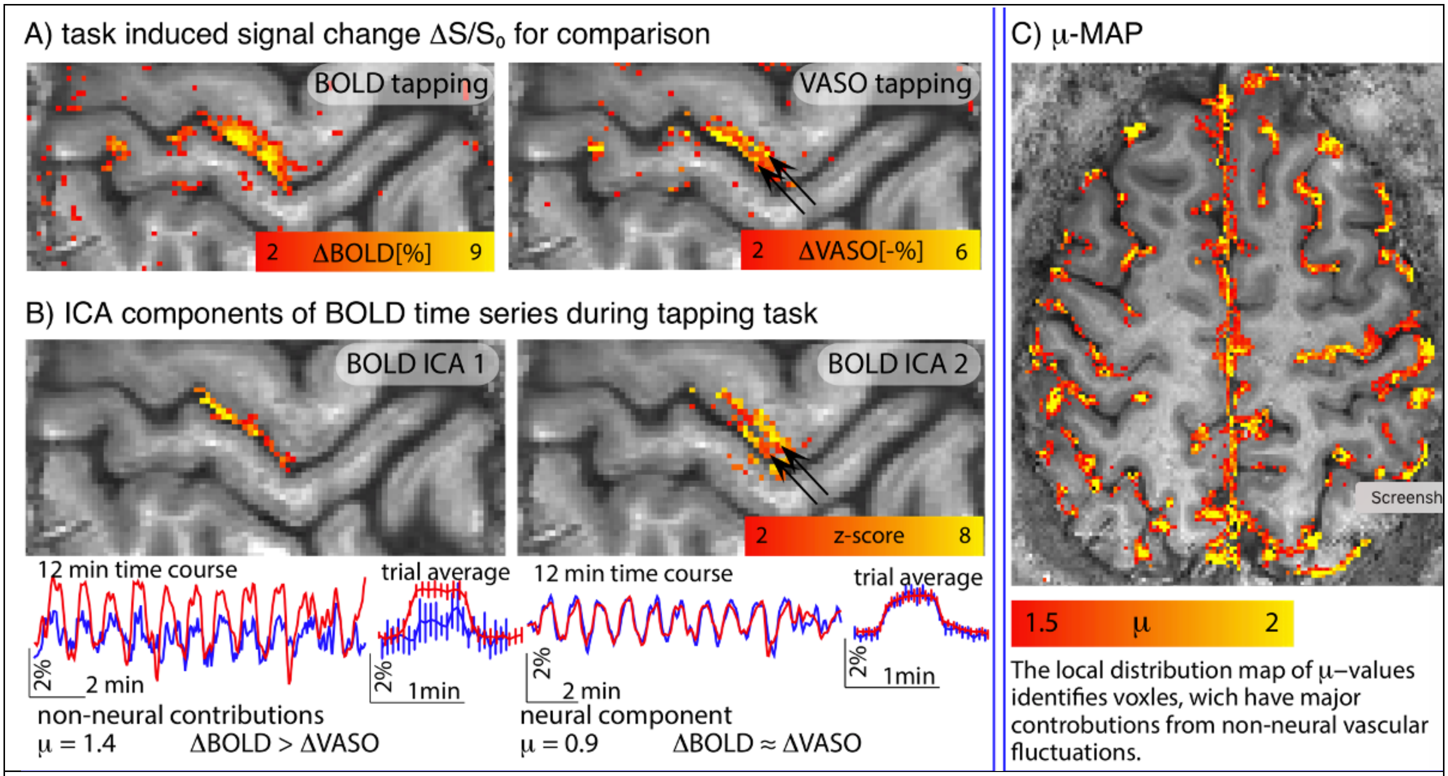

Figure 9: A) Simultaneously obtained activation maps in motor cortex corresponding to a finger tapping task. B) BOLD ICA components derived from the activation time series. At bottom are the BOLD and VASO time series for the venous ICA component and the layer-specific ICA component, showing the difference in ratios. C) A map of BOLD to VASO ratios, mapping the high ratios and showing that they correspond clearly to regions of sulci where the larger vessels reside.

Using VAPER to Probe Visual – Auditory Activation in Planum Temporale

Perfusion contrasts using arterial spin-labeling have comparable specificity to VASO, however their sensitivity is lower, preventing their use for layer fMRI. We developed a pulse sequence named VAPER (integrated VASO and PERfusion), which uses DANTE (Delay Alternating with Nutation for Tailored Excitation)[16] pulses for both nulling blood (blood volume contrast) and tagging blood (perfusion contrast)[4]. During DANTE pulses, blood signal in the microvasculature is nearly nulled to achieve a VASO contrast. After DANTE, fresh blood from outside of the coil coverage flows into the image microvasculature and replaces the nulled blood, generating a perfusion contrast. The signal difference between during-blood suppression and after-blood suppression conditions forms an integrated VASO and perfusion contrast. Both contrasts are sensitive to the microvasculature and add to increase sensitivity. Because no waiting period is needed for the blood to pass through the null point, this approach is more time efficient and therefore allows greater brain coverage per unit time. We demonstrate the use of this sequence below.

Multisensory integration can occur in areas such as the planum temporale (PT) that are commonly considered unisensory. Feedforward vs. feedback projections to the PT for multisensory processing are not well understood. The aim of the current study was to explore the laminar activity pattern in different subfields of human PT under unimodal and multisensory stimulation conditions. To this end, we acquired BOLD and VAPER contrast concurrently during a combined visual and auditory task. The stimulus consisted of a visual display of a left-right moving object and an accompanying stereo sound that moved with the object position in the visual field. Runs included combined audio-visual stimuli, and separate unimodal stimuli. Results are shown in Figure 10. The anterior PT was activated more by auditory input, as shown in Figure 10A, and it received feedback modulation in superficial layers as shown in Figure 10B. The high amplitude of pure audio input appears attenuated by the combined audiovisual input, as further shown in the subtraction plot in Figure 10B. This feedback projection is hypothesized to come through a top-down process from high order multimodal areas. The posterior PT was activated more by visual input, showing activation in both superficial and deep layers (not shown). This feedback projection is likely from the visual cortex directly. *{Within SFIM: Yuhui Chai, Arman Khojandi, Daniel Handwerker. Outside of SFIM: Tina Liu, Sean Marrett, Linqing Li, Arjen Alink, Lars Muckli}*

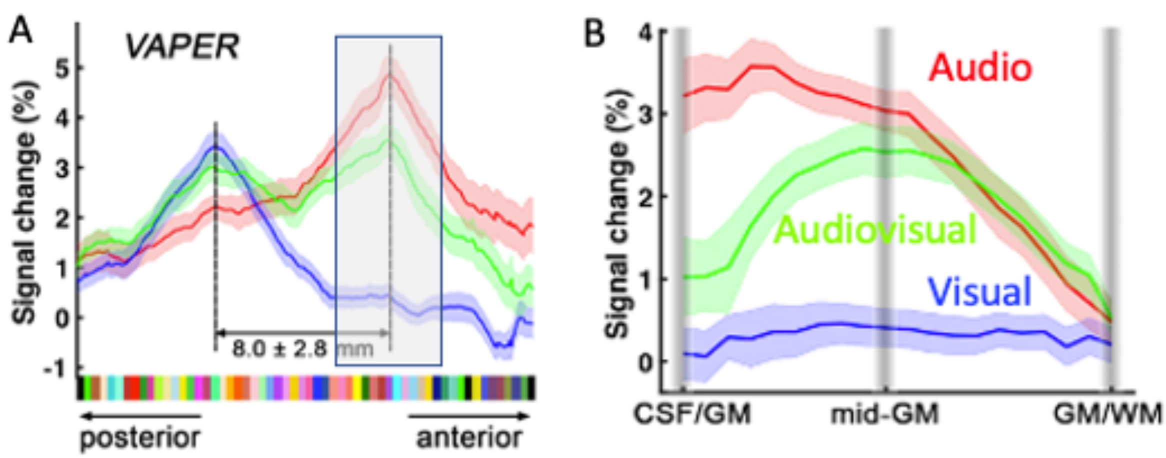

Figure 10: Activation along the planum temporale and across layers in the anterior planum temporale. A) Group-averaged columnar profiles of sensory representations using VAPER contrast along the planum temporale. Blue, red and green curves represent signal changes in BOLD and VAPER: visual-only (blue), auditory-only (red) and audiovisual stimuli (green). The distance between peaks of auditory and visual representations is 8 ± 2.8 mm along the cortical curvature. B) The layer profile from the gray boxed area in A. Laminar profile for VAPER response to the stimuli of different sensory modalities. In superficial layers, the audiovisual response shows attenuation relative to the audio only response.

Using Layer-fMRI for Whole Brain Functional Connectome Studies

Almost all layer-fMRI studies to date have focused on specific cortical regions. For layer-fMRI to reach its full potential, brain-wide laminar maps of either activation or connectivity need to be obtained. VASO is sensitive to blood volume changes, which as mentioned above, provides an optimal combination of specificity and sensitivity. While VASO was originally proposed as a blood-nulling method, it has in the last 15 years been generalized to a general T1- contrast without specific blood-nulling requirements. The general VASO strategy was generalized to extract CBV changes at any inversion time[17,18]. This literature has shown that blood-nulling is not the only way of obtaining a CBV-weighting. In fact, as long as there is a different T1 weighting between the extravascular signal and intravascular signal, any volume redistribution between these pools of z magnetization will result in a VASO signal change. Thus, instead of using an inversion pulse, T1 weighting can also be introduced by variable flip angles that create a dynamic steady-state across k-space segments along the 3D-EPI trajectory. This approach has the advantage that the T1 weighting can be maintained in a dynamic equilibrium for as long as needed. Analogously to the MAGIC VASO method [19], with multiple inversion pulses, the variable flip angle approach is called Multiple Acquisitions with Global Excitation Cycling (MAGEC) VASO. Since MAGEC VASO does not rely on a given inversion time, the readout can be prolonged as much as needed (at the cost of TR). This allows for increased coverage with up to 72–104 slices at 0.8 mm isotropic resolution and with TR of 6.5–8s. Since the blood z-magnetization is not completely nulled, the MAGEC approach may contain cerebral blood flow (CBF) dependent VASO signal amplification. Since CBF is believed to be dominated by capillary water exchange only, this will not compromise the layer-specificity. Rather, it improves the sensitivity. As long as there is a reference image acquired without this T1-weighting, the T1-related signal changes can be separated from T2* related signal changes to extract CBV signal without BOLD contamination.

Using this pulse sequence, we extended the coverage to include almost the entire brain[7]. These data have been used to explore novel avenues to investigating resting-state connectivity and provided whole brain layer-dependent connectome matrices. Figure 11 shows the explosion of data with the added dimension of cortical depth. Often, for connectivity studies, the brain is segmented, and the connectivity from every segment to every other segment is displayed in a connectivity matrix (Figure 11B). Now each matrix element can be expanded to a layer profile connectivity matrix, creating a wealth of information yet a challenging opportunity in terms of both computation and precise interpretation (Figure 11C and D). *{Within SFIM: Laurentius Huber, Emily Finn, Yuhui Chai. Outside of SFIM: Rainer Goebel, Rudiger Stirnberg, Tony Stocker, Kamil Uludag, Seong-Gi Kim, SoHyuan Han, Benedikt Poser}*

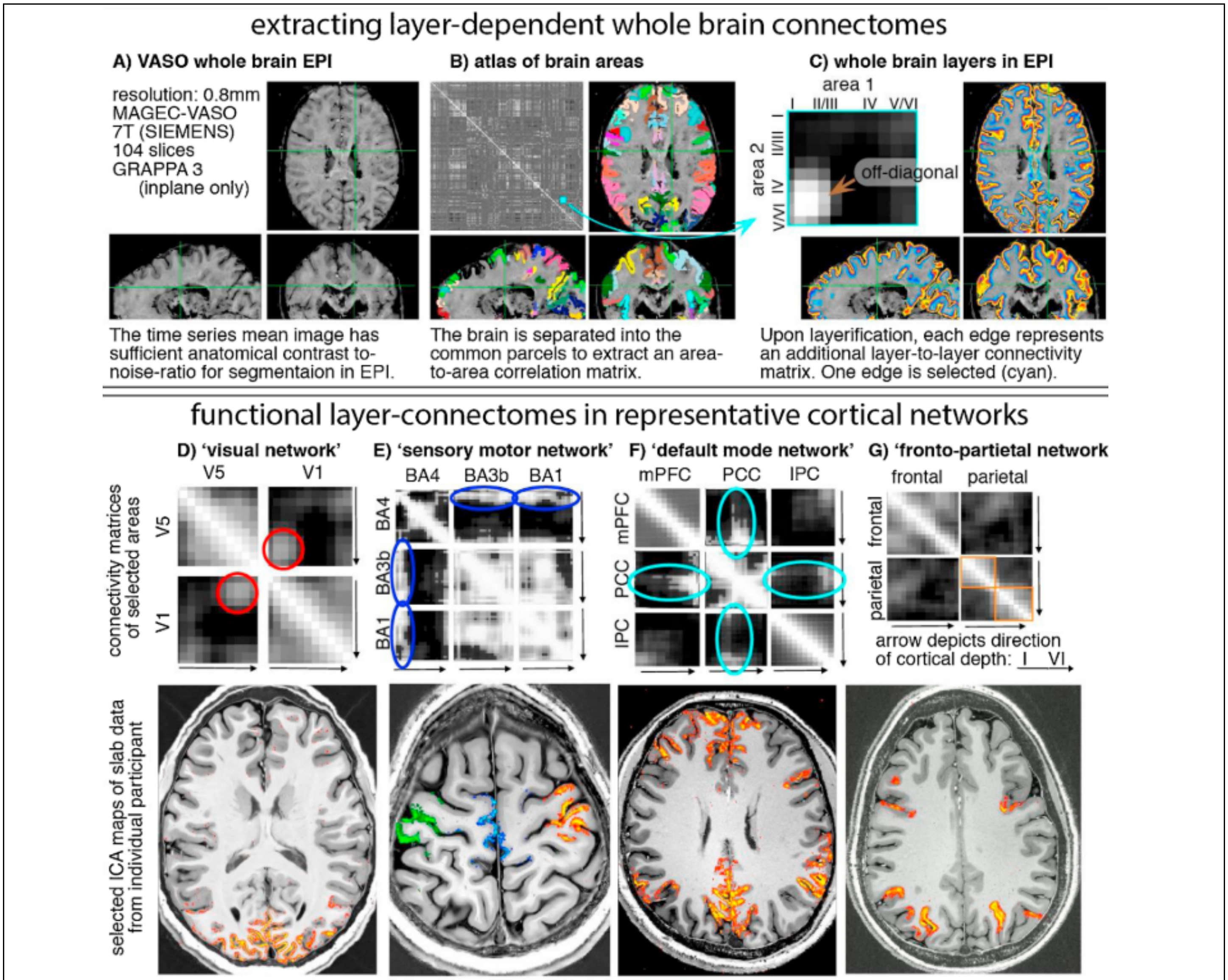

Figure 11: Whole-brain layer-dependent connectome mapping. This figure shows a possible analysis approach and representative example data to exemplify what kind of information layer-fMRI can contribute to interpret the brain's connectome. A) depicts the raw VASO EPI data quality for whole-brain layer-dependent connectomics. B) illustrates how functional connectome matrices are commonly generated: First, the brain is parcellated into a number of brain areas (colored masks overlaid on brain refer to the Shen (2013) atlas). Then, the average time courses within each brain area correlated against all other brain area's time courses. The combinations of all correlation values are summarized in a functional connectivity matrix. Any value refers to one edge of the brain

connectome and represents the functional connectivity strength between two brain areas. C) shows that the resolution of layer-fMRI can add an additional dimension in connectome analyses. Since each brain area can be subdivided into multiple layers (colored masks overlaid on the brain), each node in the whole-brain connectivity matrix represents a layer-to-layer connectivity matrix in itself. One example node is highlighted (cyan). Here, rows and columns refer to layers. Superficial layers are depicted at the top and on the left, while the deeper layers are depicted on the bottom and on the right. Off-diagonal elements can be used to interpret directional connectivity. High connectivity values on the bottom left suggest that the connectivity is dominated from connections between middle/deeper layers of area 2 and superficial layers in area 1. Area 1 sends input into feed-forward layers of area 2, while area 2 send feedback input to area 1 in the superficial layers. D–G) depict representative layer-dependent connectivities of common large networks. D) depicts the 'visual network'. Selected correlation diagrams between V1 and V5/hMT+ confirm data from Fig. 4D. Namely, V1 receives top-down feedback in superficial layers from V5, while V5 receives bottom-up input in the middle/deeper layers (red circles). Panel E) depicts the 'sensory motor network'. As expected from previous layer-fMRI studies, the primary motor cortex receives input from the sensory areas solely in superficial layers (dark blue ellipses). Panel F) shows an example of the 'default mode network'. Cyan ellipses highlight that the PCC is the only middle-layer dominated ROI. The other ROIs seem to be more feedback driven. This can be taken as an indication that the PCC is the major hub of the 'default mode network', while the other areas are being passively driven perhaps by PCC activity. Panel G) depicts the 'fronto-parietal network'. Orange squares depict how the superficial and deeper layers have strong within-region connectivity and weak connectivity between each other. They almost look like two independent brain areas. This is consistent with electrophysiology data previously presented in monkeys.

Understanding and Leveraging Time Series Information

In this second section, we addressed the challenge of leveraging more information from the transients and fluctuations in time series data. Our approach was to look beyond linear models using task timing-based regressors and beyond stationary assumptions on resting state time series data. Rather we designed approaches that used resting state and naturalistic stimuli and then employed cross subject correlation, sliding window correlation, and deconvolution to characterize of temporal/spatial features. These provided novel information about ongoing spontaneous or naturalistic stimuli-driven processes as well as revealing previously undetected features related to individual traits relative to others.

In ongoing work, we demonstrated that neural correlates of reading ability are able to be derived using written and verbal narratives combined with inter-subject correlation analysis. We further extended our cross-time series correlation approach to determine how brain states of subjects change during repeated identical movie viewing. We also applied cross subject time series analysis to EEG data to find clear differences in cross subject coherence between monozygotic and dizygotic twins. Further, we demonstrated our latest insights into the use of fMRI time series-based measures of vigilance. Lastly, we demonstrated the novel application of multivariate decoding in event-related activation, where we showed that accurate decoding occurs early in the hemodynamic response - prior to the event-related response peak, suggesting that this approach is less influenced by delayed venous responses, thus increasing the temporal precision of fMRI.

Completed work

Spontaneous thought assessment by dimensionality reduction and deconvolution

The field of brain functional connectomics studies how distributed brain regions interact to support cognition. Informative functional connectivity dynamics have been observed at the scale of seconds to minutes. Using methods previously tested on multi-task datasets[20], we were able to demonstrate that resting dynamic functional connectivity is influenced by short periods of spontaneous cognitive-task-like processes, and that the nature of the cognitive processes can be inferred from the data without knowledge of the activation timing[21]. This work demonstrates that behaviorally relevant whole-brain functional connectivity (FC) configurations are detectable and mappable during both task and resting-state scans. It also demonstrates the utility of dimensionality reduction approaches (e.g. Laplacian Embeddings) as a means to bring functional connectivity matrices into low dimensional spaces (e.g. 3D) that are easy to visualize and can facilitate tracking behaviorally meaningful connectivity dynamics. Figure 12 summarizes the methods involved. In this figure, we show our dual approach. First, we rely on a sliding window correlation and k-means clustering to temporally segment scans into periods that show consistent connectivity. Next, we rely on BOLD deconvolution[22] to generate activity maps per segment of interest despite lacking timing information regarding subjects' behavior inside the scanner. The clustering algorithm was successful in blindly grouping scan periods corresponding to distinct tasks (rest, memory, video, math) in the multi-task dataset. Similarly, when deconvolved maps were averaged within each detected segment and spatially compared against an existing comprehensive database of activation maps provided by Neurosynth (neurosynth.org), we were able to accurately draw inferences about the most likely mental activity taking place during each scan segment. Figure 13A through I show how the strongest associations of deconvolved maps occur for cognitive concepts (derived from comparison to Neurosynth maps) that best describe the tasks subjects were performing during a given scan segment. Figure 13J shows our results in a group study where we applied the same algorithm to resting state data. The pie chart shows the percentage of time that each identified topic, grouped by cognitive domain, is marked as having a strong association with the deconvolved activity maps

Ideally, if a library of *connectivity* profiles associated with cognitive states existed, it would allow us to bypass the deconvolution and Neurosynth comparison steps. We intent to start building such a database. In addition, we are also working on the goal of developing methods for objectively obtaining during and post-scan information from individual subject to more objectively characterize their ongoing cognitive state, for comparison. *{Within SFIM: Javier Gonzalez-Castillo, Natasha Topolski, Daniel Handwerker, Outside of SFIM: Cesar Caballero-Gaudes}*

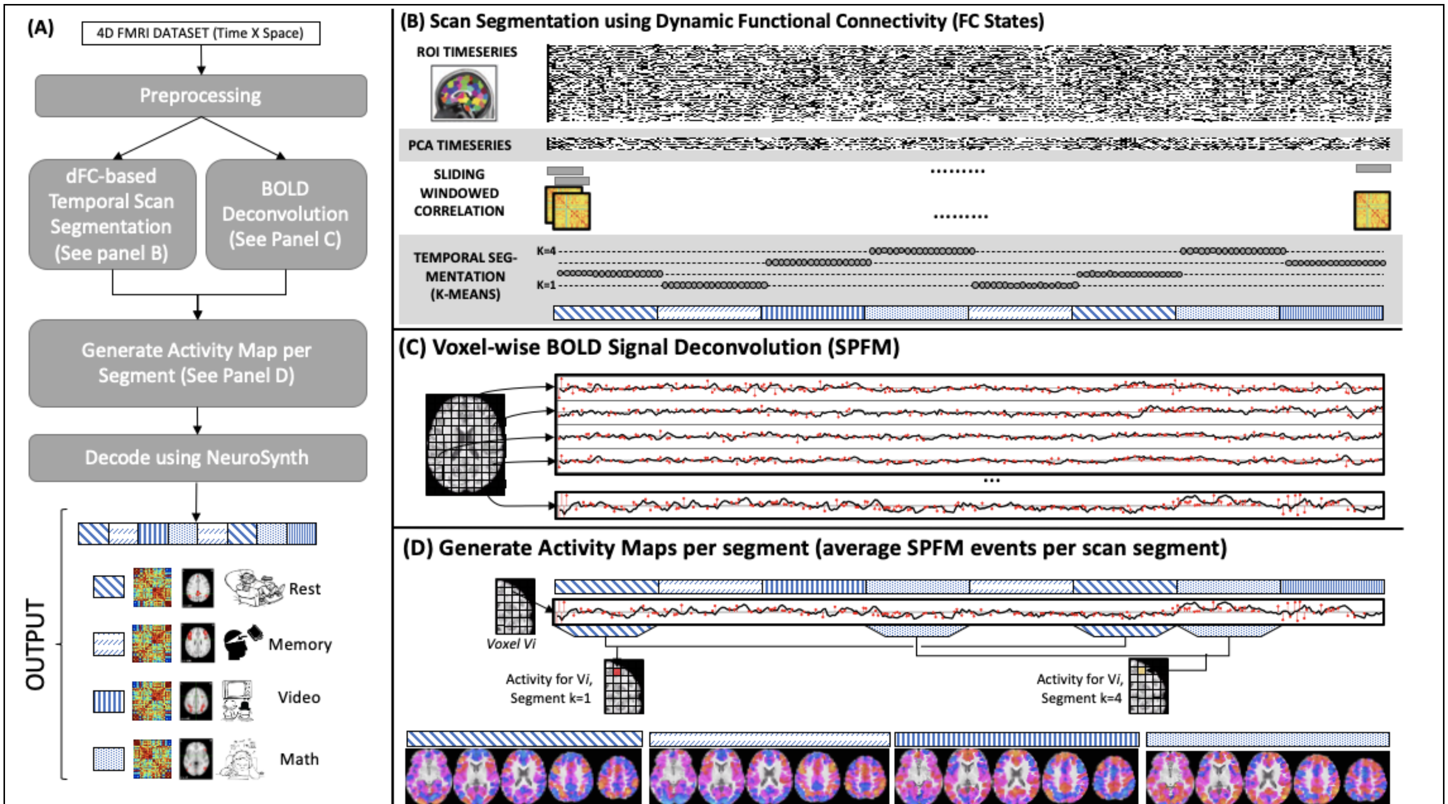

Figure 12: Schematic depiction of the analysis pipeline. (A) High level start-to-end schematic of analyses for the segmentation and decoding of task periods in the multi-task dataset. (B) Depiction of the main steps involved in the scan segmentation portion of the analyses. Following pre-processing, representative time series were obtained for all ROIs and those were inputted to a PCA step to reduce the dimensionality of the data. The next step was to compute sliding windowed correlation matrixes that were subsequently entered into a k-means analysis to assign each window to one of four segments. (C) Deconvolution was performed at the voxel-wise level. For each voxel, the deconvolution algorithm takes a pre-processed timeseries (black curve) as an input and produces as output a time series of sparse events (red stems). (D) Activation maps per segment were generated by averaging event time series (red) within the confines of each segment as determined by the k-means step (blocks with same filling patterns). After completing this operation on each voxel, a full brain activity map was obtained per scan segment (bottom of panel D).

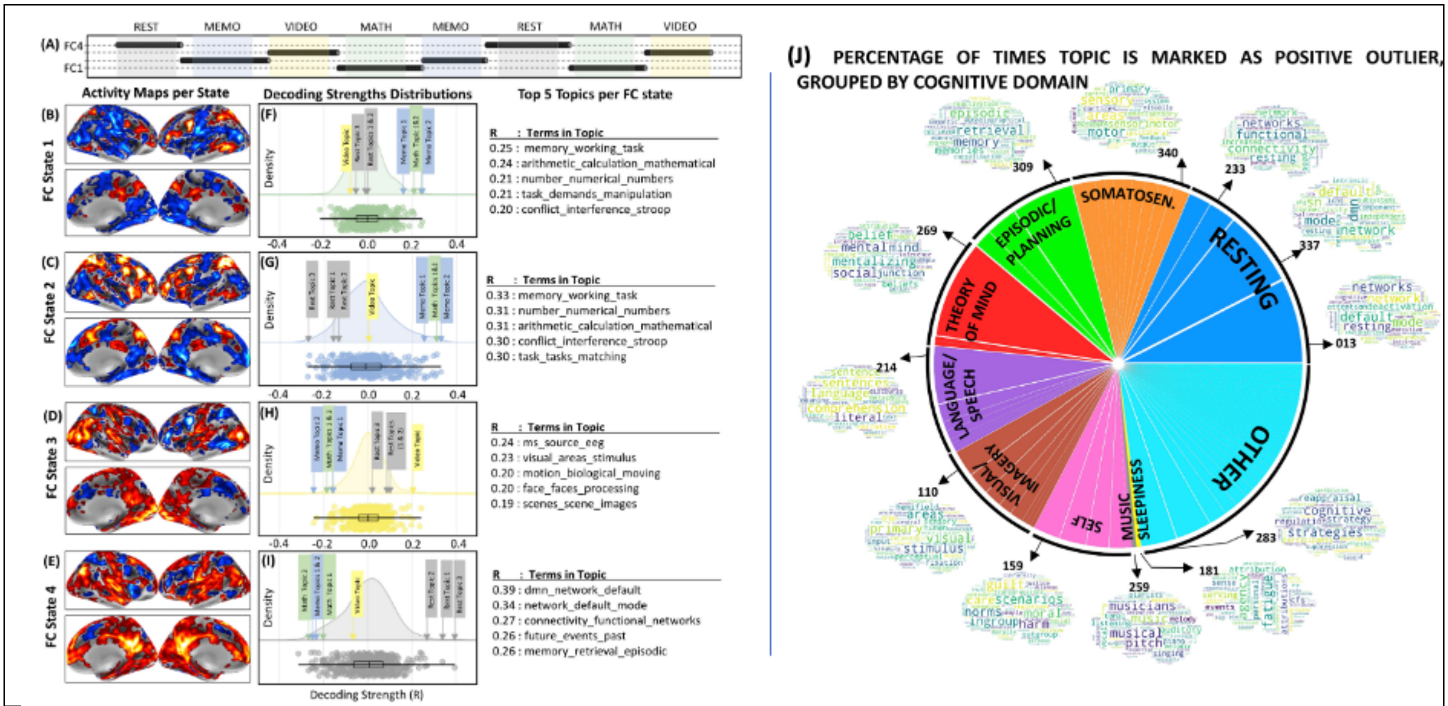

Figure 13: Individual subject task decoding results for multi-task (A-I) and resting state data (J) when comparing against the Neurosynth 400-topics set. A) Scan segmentation results. Each dot represents a snapshot of windowed connectivity. The position of the dot in the y-axis indicates to which FC-state the snapshot of windowed connectivity was assigned. Tasks periods are depicted as colored bands for reference (REST: grey; MEMO: blue; MATH: green; VIDEO: yellow). B–E) Activity maps for each FC-state obtained with Sparse Free Paradigm Mapping deconvolution algorithm. F–I) Decoding results in the form of cloud plots and top-five lists. Cloud plots depict the probability distribution of decoding strength values across all 400 topics for each FC state in the form of kernel density estimates (colored curves), swarm plots (colored dots; one per topic) and boxplots (black). In these plots the location of "correct" topics per task are clearly marked by boxed text with arrows. Finally, the tables on the right of the figure lists the top 5 topics with the highest decoding strength for each FC state. Topic names are constructed using the top three terms associated with the topic. J) Depiction of the distribution of outlier topics for spoke-like structures in the pure rest scenario grouped by cognitive domains previously reported to describe the most common cognitive processes that subjects engage with during rest.

Deriving Individual Information from Naturalistic Stimuli

Traditional task-based fMRI experiments use tightly controlled paradigms that often lack ecological validity; resting-state scans, on the other hand, are entirely unconstrained, making it difficult to separate signal from noise. Naturalistic tasks, in which subjects view a movie or listen to a story in the scanner, may provide a happy medium for studying both group-level functional brain organization as well as individual differences. By imposing a standardized yet engaging stimulus on all subjects, naturalistic tasks evoke rich patterns of brain activity. These patterns lend themselves to flexible, data-driven analyses such as ISC[23], which is a model-free way to isolate stimulus-dependent brain activity from spontaneous activity and noise. Because these approaches rely on activity that is time-locked across individuals, they cannot be applied to resting-state data. These techniques have several advantages over traditional approaches: 1) they do not require *a priori* modeling of specific task events and/or assumptions about the functional specificity of individual brain regions; 2) there is no need to assume a fixed hemodynamic response function; and 3) they allow for the characterization of the full spatiotemporal richness of both evoked and intrinsic brain activity.

We use a novel technique called inter-subject representational similarity analysis (IS-RSA), which adapts ISC to highlight stimulus-driven responses that are idiosyncratic rather than shared to extract individual information from naturalistic fMRI data[24]. We have shown that it can recover brain-behavior relationships while people watch complex, engaging videos. Using a publicly available dataset with n = 184 subjects watching movie clips during high-resolution fMRI, we have shown that IS-RSA is sensitive to both cognitive and social/affective traits, as well as differences in the similarity structure between brain and behavioral data for different traits. For example, individuals who score high on a test of working memory (an indicator of trait cognitive ability) show more similar brain responses while watching movies, while low scorers are more variable, in that their brain responses look less similar to one another, as well as to those of high scorers, as shown in Figure 14A. On the other hand, people with more similar personalities (as determined by the questionnaires), regardless of absolute levels of individual traits, show more similar brain responses across several parts of cortex, as shown in Figure 14B, especially while watching video clips containing social information. We are continuing to develop and refine this method to understand which features of the videos trigger trait-dependent responses, with the ultimate goal of developing a brain-based "stress test" that is more sensitive to individual differences in behavior than either resting state or traditional psychological tasks.

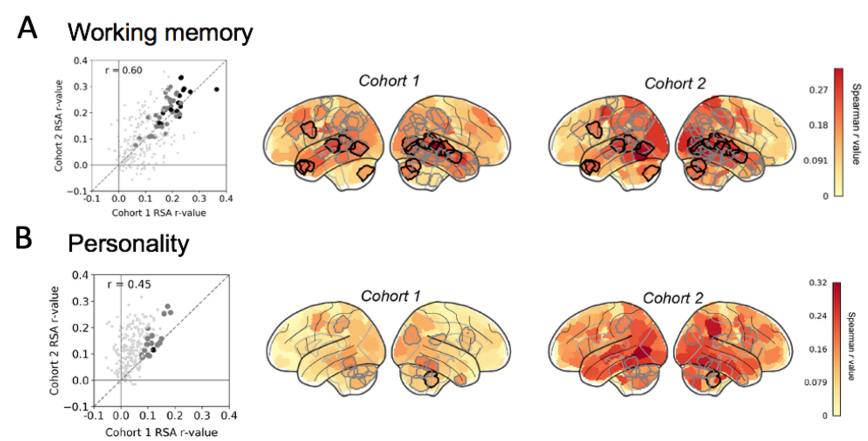

Figure 14: Do pairs of subjects that score more similarly on behavioral traits also show stronger ISC in certain brain regions during naturalistic viewing? Two traits are tested: working memory ability (A) and personality (B). In the scatter plots, each dot represents one node in a whole-brain atlas (268 total), plotted according to its representational similarity between brain and behavior in cohort 1 (n = 93 unrelated subjects; x-axis) versus its representational similarity in cohort 2 (n = 89 unrelated subjects; y-axis). **Large gray dots** are nodes that show significant representational similarity ($p < 0.05$, uncorrected) after permutation testing in both cohorts (no. permutations = 10,000 for each cohort); **large black dots** are nodes that show significant representational similarity ($p < 0.05$) after Bonferroni-style correction. Glass brains show nodes colored by IS-RSA value. Nodes outlined in gray and black show significant representational similarity. The two-cohort approach was used to avoid calculating brain or behavioral similarity between related pairs of subjects, and also to test for replicability and generalizability of results.

In a direct comparison of acquisition type (naturalistic versus rest) using functional connectivity-based methods, we have shown that movie data is superior to resting-state data for the prediction of individual traits. Functional connectivity data from specific movie clips as short as 1-2 minutes are sufficient to predict both cognitive ability (up to $r = 0.38$ for most successful clip) and emotional traits (up to $r = 0.24$), in some cases with equal or higher accuracy than using a full 15-min resting state run, suggesting that these clips contain certain content or other features that amplify meaningful individual differences in connectivity[25]. Using automated semantic labels, we related semantic content of each clip to its predictive accuracy and found that clips containing more human content yielded more accurate predictions of cognitive ability. Relatedly, clips that had a higher percentage of timepoints with faces onscreen tended to perform better for predicting cognitive ability ($r = 0.69$, $p = 0.009$), again suggesting that social content is particularly effective for eliciting meaningful individual differences in connectivity. These results suggest that naturalistic movie-watching data is more sensitive to individual differences than rest, and that short naturalistic acquisitions can be used to build models that generalize to predict behavior in unseen subjects. *{Within SFIM: Emily Finn, Peter Molfese, Daniel Handwerker, Arman Khojandi. Outside of SFIM: Enrico Glerean, Dylan Nielson}*

Trait Paranoia Shapes Inter-Subject Synchrony

Individuals often interpret the same event in different ways. How do personality traits modulate brain activity evoked by a complex stimulus? Here we report results from a naturalistic paradigm designed to draw out both neural and behavioral variation along a specific dimension of interest, namely paranoia[26]. Participants listen to a narrative during functional MRI describing an ambiguous social scenario, written such that some individuals would find it highly suspicious, while others less so. Using ISC analysis, we first identified multiple cortical areas that were activated by narrative listening. We then identified several brain areas that are differentially synchronized during listening between participants with high and low trait-level paranoia, including theory-of-mind regions. Follow-up analyses indicate that these regions are more active to mentalizing events in high-paranoia individuals. Analyzing participants' speech as they freely recall the narrative reveals semantic and syntactic features that also scale with paranoia. Results indicate that a personality trait can act as an intrinsic "prime," yielding different neural and behavioral responses to the same stimulus across individuals. *{Within SFIM: Emily Finn. Outside of SFIM: Philip Corlett, Gang Chen, R. Todd Constable}*

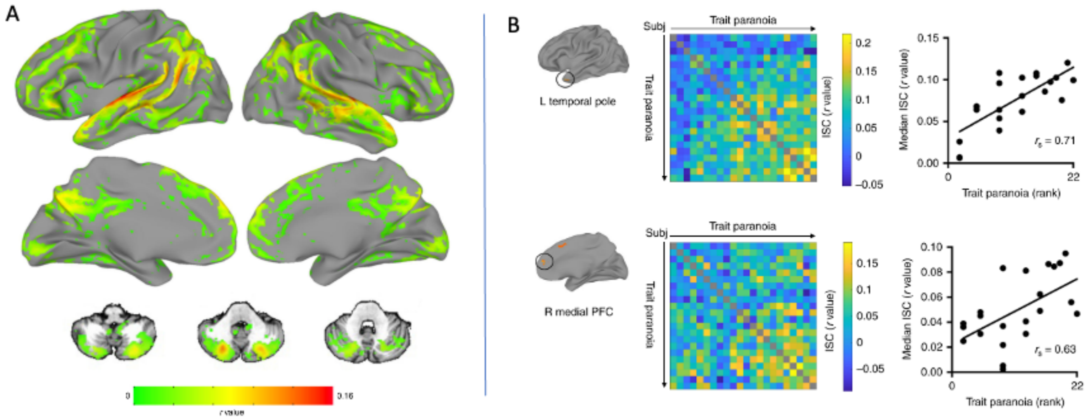

Figure 15: A) Narrative listening evokes widespread inter-subject correlation (ISC) across the whole sample. Voxels showing significant ISC across the time course of narrative listening in all participants (n = 22). As expected, the highest ISC values were observed in the auditory cortex, but several regions of association cortex in the temporal, parietal, frontal, and cingulate lobes as well as the cerebellum also showed high synchrony. Results are displayed at a voxel-wise false-discovery rate (FDR) threshold of q < 0.001. B) Inter-subject correlation (ISC) scales continuously with trait paranoia. Post-hoc analyses for two regions of interest (ROIs) that emerged from the dichotomized contrast between high- and low-paranoia groups: left temporal pole (top) and right medial prefrontal cortex (PFC, bottom). Participants are ordered by increasing trait paranoia score. Each matrix element reflects the correlation between two participants' activation time courses in the left temporal pole during narrative listening. Higher correlations are visible as one moves to the right and down along the diagonal, representing pairs of increasingly high-paranoia individuals. Also shown are scatter plots of paranoia rank vs. median ISC value.

Ongoing Work

Inter-Subject Correlation During Narratives Reveals Reading Ability

The neuroscience of reading has recently been extended to the study of individual differences, with certain regions appearing differently activated in dyslexic or struggling readers. Recent work using ISC analysis suggests that a longer narrative has a reliable effect on the fMRI response to movie and story stimuli, especially in frontal regions not activated by typically used randomized words and phrases[27]. In this study, we presented coherent stories to adolescents having a wide range of reading abilities. The stories were presented in alternating visual and auditory blocks. We used a two-group ISC analysis to identify regions in which good and poor readers had different levels of consistency with other readers during these narratives. This analysis identified a widespread set of brain regions, shown in Figure 16, in which good readers had activity time courses that were more similar to each other than poor readers. These group differences were not visible with standard block analyses. Poor readers had more "idiosyncratic" and generally lower correlations with both good and other poor readers, suggesting a range of compensatory mechanisms. These differences were not explained by IQ, age, or motion. These results suggest an expansion of the current view of where and how the brain is affected by reading ability, and establishe ISC as a sensitive tool for future studies of reading disorders. *{Within SFIM: David Jangraw, Emily Finn, Peter Molfese. Outside of SFIM: Nicole Landi, Fumiko Hoeft, Stephen Frost, Kenneth Pugh}*

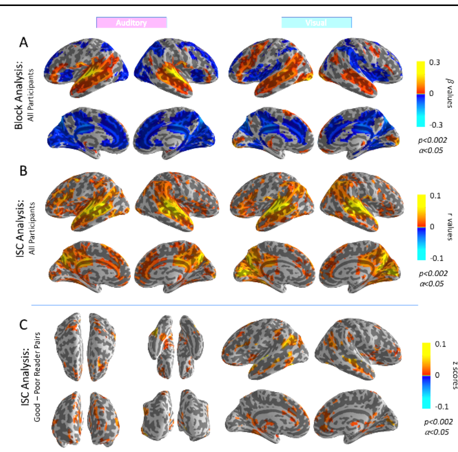

Figure 16: Task-related activation (A) and ISC (B) for the Auditory (left) and Visual (right) narrative task. Much of the brain shows task-related activation changes in response to both modalities. C) Differences between good and poor readers. ISC Analysis results show a number of larger areas where ISC across the entire run was greater among good reader pairs than among poor reader pairs. Block analyses (not shown) showed no significant group differences.

Decoding Cognitive States During Repeated Movie Viewing

In our previously mentioned study, we used sliding window dynamic connectivity to identify and decode mental states (see "Spontaneous thought assessment by dimensionality reduction and deconvolution"). Here, we used the same method to explore the consistency of mental states across repeated (16 trials) viewing of the identical movie. In our analysis, we performed sliding window correlation on time series from a parcellated brain. We then applied dimensionality reduction to characterize the 3D trajectory of connectivity profile of each time series. We then calculated the Euclidian distance at each time point between each time series vector projection to determine the similarity between repeated runs and time points. Figure 17 shows the median Euclidian distance between all pairs of runs for 16 sequential views of the identical movie. First it is clear from the slope that as the movie continues, the difference between runs grows, suggesting a drift in consistency of cognitive state. Secondly, there are several consistent time periods during the runs where the similarity briefly increases. These periods are hypothesized to be points where the subject's attention was engaged by emotional or otherwise significant moments in the movie. Inspection of the segments reveals that indeed these moments were when the main characters in the movie were initiating clear actions and emotions. This analysis approach lends itself well to characterizing salient periods in naturalistic stimuli as well as characterizing subject engagement over time. It also may help guide future paradigm design or analysis that leverages these moments of increased similarity. *{Within SFIM: Ramya Varadarajan, Daniel Handwerker, Javier Gonzalez-Castillo}*

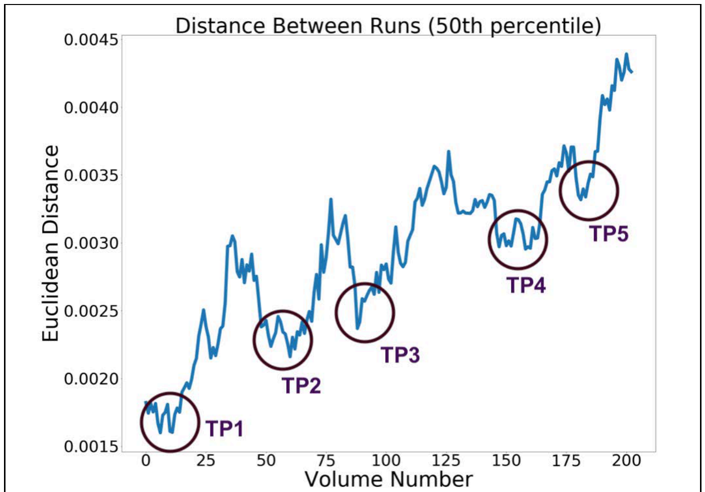

Figure 17: At every time point, we calculated the Euclidean distance between every pair of runs. This plot shows the median Euclidean distance between runs at each time point. The five local minima on the figure, circled, represent time periods (TPs) during which median Euclidean distances are relatively low, meaning that the pattern brain activation is more similar between runs.

EEG Brain Synchrony Differences in Mono vs Dizygotic Twins

As shown above, ISC methods have been found to be useful for relating brain synchrony to traits in individual subjects. In the current work, we attempt to use ISC to identify similarities and differences between monozygotic (MZ) and dizygotic (DZ) twins using EEG/ERP data.

These data reflect 19 twin pairs (38 participants total; 8 pairs MZ, 11 pairs DZ) who participated in this study over three time points: at age 6 months, 12 months, and 18 months. At each time point, infants were presented with auditory stimuli that included six Consonant-Vowel (CV) syllables: /ba/ /da/ /ga/ /bu/ /du/ /gu/. EEG data were recorded using 128-electrode array (EGI/Philips Neuro) at 250Hz, bandpass filter 0.1-30Hz. Data were average-referenced, baseline corrected, and averaged to form ERPs. All participants supplied at least 15 trials per average out of a possible 25 total trials per category. An inter-subject correlation analysis was performed which determined the correlation between electrode waveforms as matched pairs (MZ vs. DZ) or random assignment. Statistical significance was assessed using a modified linear-mixed effects model. As shown in Figure 18, ISC analyses identified several significant clusters present in MZ twins which were not apparent in DZ twins, or in

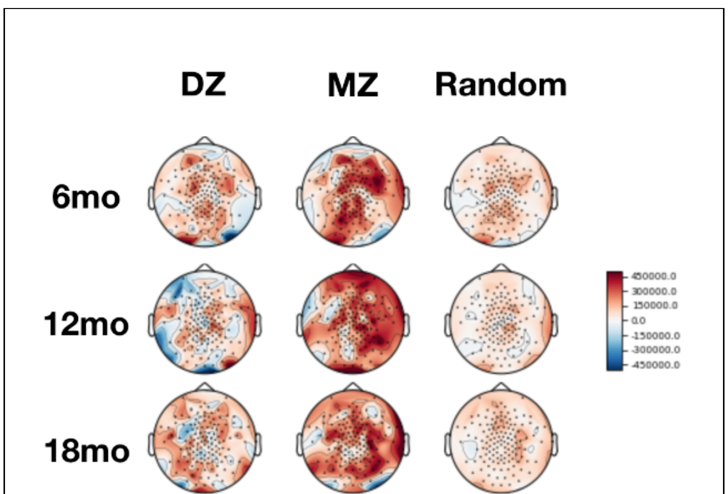

Figure 18: Inter-subject correlation of ERPs reveals higher synchrony in monozygotic (MZ) twins compared to dizygotic (DZ) twins or to randomly paired non-related subjects.

analysis pairing infants with other unrelated participants, corrected for whole-head significance. Much like in fMRI, ISC is a novel and potentially powerful method for identifying shared variance between participants in EEG. In particular, ISC allows for finer-grained identification of sensor-space similarities and differences compared to traditional methods (e.g. peak-amplitude), including data-driven methods like PCA. *{Within SFIM: Peter Molfese, Emily Finn. Outside of SFIM: Dennis Molfese, Victoria Molfese}*

Data-driven Estimation of Vigilance and Wakefulness in Resting-state fMRI

Shifts in vigilance and wakefulness constitute an important confound in the study of dynamic functional connectivity[28]. It is currently challenging to identify these shifts without external measures. Previous studies have demonstrated that traces of wakefulness and vigilance are present in different aspects of the fMRI data, including the global signal and ultra-slow fluctuations in lower CSF compartments (e.g., 4th ventricle)[29]. The purpose of this ongoing work was to evaluate ways to derive a continuous measure of vigilance from the fMRI data by combining these metrics. In our preliminary studies, shown in Figure 19, we have confirmed previously published results but also have extended some observations. First, we confirmed previous findings that the amplitude of the 0.05 Hz fluctuations temporally correlate with periods of drowsiness, as suggested by our pupillometry measures – which also indicated when eyes were closed. Also, as found in previous studies, but clearly mapped here, we find that these fluctuations are precisely anticorrelated with BOLD signal throughout large portions of gray matter. Lastly, we found, using multi-echo EPI, evidence that the sources of the fluctuations in the 4th ventricle contain BOLD-weighted signal, and thus may represent more than just CSF inflow as suggested in previous literature[29]. It is thought that these may bear some relation to the 0.03 Hz "quasi-periodic patterns" found previously[30]. *{Within SFIM: Javier Gonzalez-Castillo, Dan Handwerker, Isabel Fernandez}*

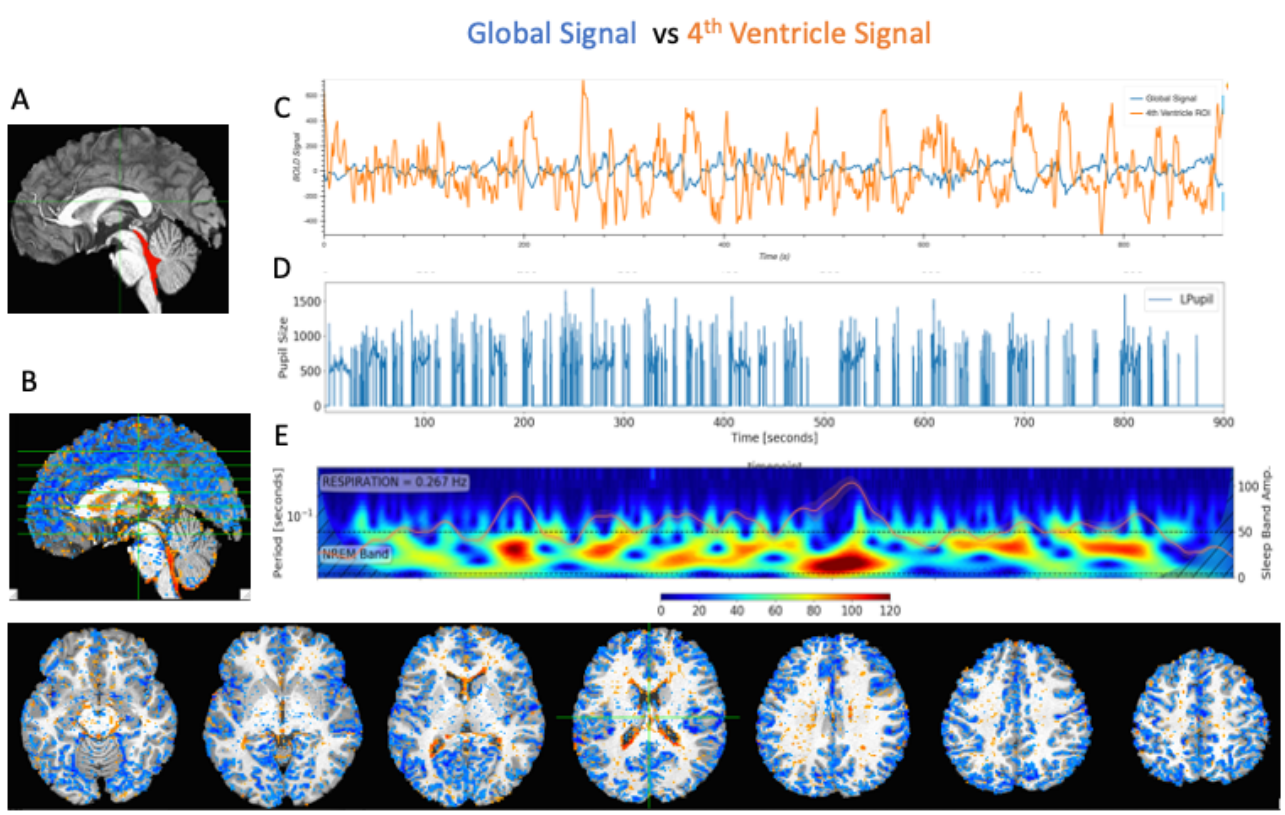

Figure 19: A) Location of ROI. B) Correlation maps from 4th ventricle regressor showing anticorrelation in most of gray matter. C) 4th Ventricle signal shows anticorrelation with global signal. D) Traces of pupil size showing when subject had eyes closed. E) Corresponding spectrograms showing when 0.05 Hz power increased – correlated with eye closure.

Rapid Event-Related Decoding

The limits of fMRI temporal resolution have been established to be limited by the sluggishness and variability in the hemodynamic response function (HRF). Specifically, the voxel-wise heterogeneity in the vasculature leads to a heterogeneity in HRF as larger, draining veins have a delayed response. The range in HRF latencies has been shown to be about 4 seconds across voxels in activated regions. Here we tested the hypothesis that the multi-voxel pattern of the early phase of the HRF, thought to be weighted towards smaller vessels, is sufficient to decode neuronal information. Specifically, we investigated the time course of decoding information by time resolved multi-voxel pattern analysis (MVPA) of rapidly sampled BOLD signals at 7 T with a TR of 125 ms. We scanned 13 healthy volunteers as they viewed images of objects. Each image was presented for 500 ms followed by a rest period for 8.5-13.5 s. BOLD signals were acquired by T2*-weighted EPI sequence with SMS factor 3 for 9 slices to cover most of the occipital and occipitotemporal areas. A decoder (linear support vector machine) was trained with the preprocessed fMRI data. Binary classification of animal vs. vehicle category was performed using a leave-one-run-out cross-validation. The training and testing of the decoder were performed at each time point.

As shown in Figure 20, the peak of hemodynamic responses for each voxel was distributed between 2-6 s, however, prediction accuracy surpassed statistical significance in less than 2 s and peaked around 4 s - significantly faster than the HRF responses time-to-peak. To examine if voxels with early latency are informative for accurate decoding, we further divided the voxels into four subgroups according to their latency and applied a decoder to each subgroup. Image category prediction was possible for all subgroups at a similar time, indicating that voxels contain information at a similar time independent of variation of hemodynamic response latency (i.e. the presence of draining veins). This was more clearly visible by comparing the time course of prediction accuracy with that of the mean hemodynamic response of each subgroup. *{Within SFIM: Yoichi Miyawaki, Daniel Handwerker, Javier Gonzalez-Castillo, Laurentius Huber, Arman Khojandi, Yuhui Chai}*

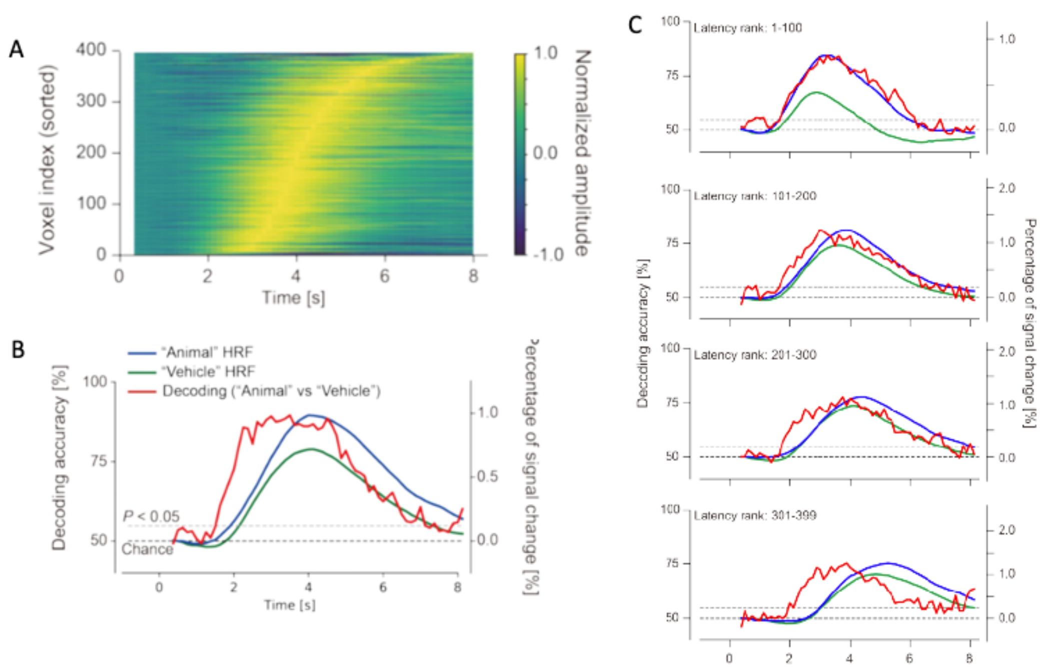

Figure 20: The hemodynamic response and the multivariate decoding time course. A) The distribution of the HRF response latency across 400 voxels in the visual cortex, showing a spread of 4 seconds. B) The time course of the averaged hemodynamic response to animals and vehicles and the corresponding multivariate decoding accuracy over time. The decoding accuracy reaches about 80% within 2 seconds, which is just as the hemodynamic response is rising from baseline. C) The timing of the decoding accuracy, shown in red, is independent of the which latency grouping of hemodynamic responses was used.

List of SFIM Publications Since Last BSC Report (44 papers, 1 book)

(Red indicates use in summary)

Gonzalez-Castillo J, Panwar P, Buchanan LC, Caballero-Gaudes C, Handwerker DA, Jangraw DC, Zachariou V, Inati S, Roopchansingh V, Derbyshire JA, et al.: **Evaluation of multi-echo ICA denoising for task based fMRI studies: Block designs, rapid event-related designs, and cardiac-gated fMRI**. *Neuroimage* 2016, **141**:452–468.

Degryse J, Seurinck R, Durnez J, Gonzalez-Castillo J, Bandettini PA, Moerkerke B: **Introducing Alternative-Based Thresholding for Defining Functional Regions of Interest in fMRI**. *Front Neurosci* 2017, **11**:222.

Gonzalez-Castillo J, Chen G, Nichols TE, Bandettini PA: **Variance decomposition for single-subject task-based fMRI activity estimates across many sessions**. *Neuroimage* 2017, **154**:206–218.

Huber L, Handwerker DA, Jangraw DC, Chen G, Hall A, Stüber C, Gonzalez-Castillo J, Ivanov D, Marrett S, Guidi M, et al.: **High-Resolution CBV-fMRI Allows Mapping of Laminar Activity and Connectivity of Cortical Input and Output in Human M1**. *Neuron* 2017, **96**:1253-1263.e7.

Kazan SM, Huber L, Flandin G, Ivanov D, Bandettini P, Weiskopf N: **Physiological basis of vascular autocalibration (VasA): Comparison to hypercapnia calibration methods**. *Magn Reson Med* 2017, **78**:1168–1173.

Keilholz S, Caballero-Gaudes C, Bandettini P, Deco G, Calhoun V: **Time-Resolved Resting-State Functional Magnetic Resonance Imaging Analysis: Current Status, Challenges, and New Directions**. *Brain Connect* 2017, **7**:465–481.

Kundu P, Voon V, Balchandani P, Lombardo M V., Poser BA, Bandettini PA: **Multi-echo fMRI: A review of applications in fMRI denoising and analysis of BOLD signals**. *Neuroimage* 2017, **154**:59–80.

Power JD, Plitt M, Kundu P, Bandettini PA, Martin A: **Temporal interpolation alters motion in fMRI scans: Magnitudes and consequences for artifact detection**. *PLoS One* 2017, **12**:e0182939.

Chai Y, Sheng J, Bandettini PA, Gao JH: **Frequency-dependent tACS modulation of BOLD signal during rhythmic visual stimulation**. *Hum Brain Mapp* 2018, **39**:2111–2120.

Finn ES, Corlett PR, Chen G, Bandettini PA, Constable RT: **Trait paranoia shapes inter-subject synchrony in brain activity during an ambiguous social narrative**. *Nat Commun* 2018, **9**:1–13.

Gonzalez-Castillo J, Bandettini PA: **Task-based dynamic functional connectivity: Recent findings and open questions**. *Neuroimage* 2018, **180**:526–533.

Huber L, Ivanov D, Handwerker DA, Marrett S, Guidi M, Uludağ K, Bandettini PA, Poser BA: **Techniques for blood volume fMRI with VASO: From low-resolution mapping towards sub-millimeter layer-dependent applications**. *Neuroimage* 2018, **164**:131–143.

Huber L, Tse DHY, Wiggins CJ, Uludağ K, Kashyap S, Jangraw DC, Bandettini PA, Poser BA, Ivanov D: **Ultra-high resolution blood volume fMRI and BOLD fMRI in humans at 9.4 T: Capabilities and challenges**. *Neuroimage* 2018, **178**:769–779.

Jangraw DC, Gonzalez-Castillo J, Handwerker DA, Ghane M, Rosenberg MD, Panwar P, Bandettini PA: **A functional connectivity-based neuromarker of sustained attention generalizes to predict recall in a reading task**. *Neuroimage* 2018, **166**:99–109.

Kundu P, Benson BE, Rosen D, Frangou S, Leibenluft E, Luh WM, Bandettini PA, Pine DS, Ernst M: **The integration of functional brain activity from adolescence to adulthood**. *J Neurosci* 2018, **38**:3559–3570.

Mcclure P, Zheng CY, Kaczmarzyk JR, Lee JA, Ghosh SS, Nielson D, Bandettini P, Pereira F: **Distributed Weight Consolidation: A Brain Segmentation Case Study**. *Adv Neural Inf Process Syst* 2018,

Power JD, Plitt M, Gotts SJ, Kundu P, Voon V, Bandettini PA, Martin A: **Ridding fMRI data of motion-related influences: Removal of signals with distinct spatial and physical bases in multiecho data**. *Proc Natl Acad Sci U S A* 2018, **115**:E2105–E2114.

Saggar M, Sporns O, Gonzalez-Castillo J, Bandettini PA, Carlsson G, Glover G, Reiss AL: **Towards a new approach to reveal dynamical organization of the brain using topological data analysis**. *Nat Commun* 2018, **9**:1–14.

Torrisi S, Chen G, Glen D, Bandettini PA, Baker CI, Reynolds R, Yen-Ting Liu J, Leshin J, Balderston N, Grillon C, et al.: **Statistical power comparisons at 3T and 7T with a GO / NOGO task**. *Neuroimage* 2018, **175**:100–110.

Xie H, Calhoun VD, Gonzalez-Castillo J, Damaraju E, Miller R, Bandettini PA, Mitra S: **Whole-brain connectivity dynamics reflect both task-specific and individual-specific modulation: A multitask study**. *Neuroimage* 2018, **180**:495–504.

Xie H, Gonzalez-Castillo J, Handwerker DA, Bandettini PA, Calhoun VD, Chen G, Damaraju E, Liu X, Mitra S: **Time-varying whole-brain functional network connectivity coupled to task engagement**. *Netw Neurosci* 2018, **3**:49–66.

Caballero-Gaudes C, Moia S, Panwar P, Bandettini PA, Gonzalez-Castillo J: **A deconvolution algorithm for multi-echo functional MRI: Multi-echo Sparse Paradigm Free Mapping**. *Neuroimage* 2019, **202**.

Chai Y, Handwerker DA, Marrett S, Gonzalez-Castillo J, Merriam EP, Hall A, Molfese PJ, Bandettini PA: **Visual temporal frequency preference shows a distinct cortical architecture using fMRI**. *Neuroimage* 2019, **197**:13–23.

Chen G, Taylor PA, Qu X, Molfese PJ, Bandettini PA, Cox RW, Finn ES: **Untangling the Relatedness among Correlations, Part III: Inter-Subject Correlation Analysis through Bayesian Multilevel Modeling for Naturalistic Scanning**. *bioRxiv* 2019, doi:10.1101/655738.

Demiral SB, Tomasi D, Sarlls J, Lee H, Wiers CE, Zehra A, Srivastava T, Ke K, Shokri-Kojori E, Freeman CR, et al.: **Apparent diffusion coefficient changes in human brain during sleep – Does it inform on the existence of a glymphatic system?** *Neuroimage* 2019, **185**:263–273.

Finn ES, Huber L, Jangraw DC, Molfese PJ, Bandettini PA: **Layer-dependent activity in human prefrontal cortex during working memory**. *Nat Neurosci* 2019, **22**:1687–1695.

Gonzalez-Castillo J, Caballero-Gaudes C, Topolski N, Handwerker DA, Pereira F, Bandettini PA: **Imaging the spontaneous flow of thought: Distinct periods of cognition contribute to dynamic functional connectivity during rest**. *Neuroimage* 2019, **202**.

Kim HC, Bandettini PA, Lee JH: **Deep neural network predicts emotional responses of the human brain from functional magnetic resonance imaging**. *Neuroimage* 2019, **186**:607–627.

McClure P, Rho N, Lee JA, Kaczmarzyk JR, Zheng CY, Ghosh SS, Nielson DM, Thomas AG, Bandettini P, Pereira F: **Knowing What You Know in Brain Segmentation Using Bayesian Deep Neural Networks**. *Front Neuroinform* 2019, **13**:67.

Xie H, Zheng CY, Handwerker DA, Bandettini PA, Calhoun VD, Mitra S, Gonzalez-Castillo J: **Efficacy of different dynamic functional connectivity methods to capture cognitively relevant information**. *Neuroimage* 2019, **188**:502–514.

Yu Y, Huber L, Yang J, Jangraw DC, Handwerker DA, Molfese PJ, Chen G, Ejima Y, Wu J, Bandettini PA: **Layer-specific activation of sensory input and predictive feedback in the human primary somatosensory cortex**. *Sci Adv* 2019, **5**:eaav9053.

Chai Y, Li L, Huber L, Poser BA, Bandettini PA: **Integrated VASO and perfusion contrast: A new tool for laminar functional MRI**. *Neuroimage* 2020, **207**:116358.

Chen G, Taylor PA, Qu X, Molfese PJ, Bandettini PA, Cox RW, Finn ES: **Untangling the relatedness among correlations, part III: Inter-subject correlation analysis through Bayesian multilevel modeling for naturalistic scanning**. *Neuroimage* 2020, **216**:116474.

Finn ES, Bandettini PA: **Movie-watching outperforms rest for functional connectivity-based prediction of behavior**. *bioRxiv* 2020, doi:10.1101/2020.08.23.263723.

Finn ES, Glerean E, Khojandi AY, Nielson D, Molfese PJ, Handwerker DA, Bandettini PA: **Idiosynchrony: From shared responses to individual differences during naturalistic neuroimaging**. *Neuroimage* 2020, **215**:116828.

Huber L (Renzo), Poser BA, Bandettini PA, Arora K, Wagstyl K, Cho S, Goense J, Nothnagel N, Morgan AT, van den Hurk J, et al.: **LAYNII: A software suite for layer-fMRI**. *bioRxiv* 2020, doi:10.1101/2020.06.12.148080.

Huber L, Finn ES, Chai Y, Goebel R, Stirnberg R, Stöcker T, Marrett S, Uludag K, Kim SG, Han SH, et al.: **Layer-dependent functional connectivity methods**. *Prog Neurobiol* 2020, doi:10.1016/j.pneurobio.2020.101835.

Huber L, Finn ES, Handwerker DA, Bönstrup M, Glen DR, Kashyap S, Ivanov D, Petridou N, Marrett S, Goense J, et al.: **Sub-millimeter fMRI reveals multiple topographical digit representations that form action maps in human motor cortex**. *Neuroimage* 2020, **208**:116463.

Jo HJ, Reynolds RC, Gotts SJ, Handwerker DA, Balzekas I, Martin A, Cox RW, Bandettini PA: **Fast detection and reduction of local transient artifacts in resting-state fMRI**. *Comput Biol Med* 2020, **120**:103742.

Yang J, Molfese PJ, Yu Y, Handwerker DA, Chen G, Taylor PA, Ejima Y, Wu J, Bandettini PA: **Different activation signatures in the primary sensorimotor and higher-level regions for haptic three-dimensional curved surface exploration**. *bioRxiv* 2020, doi:10.1101/2020.08.04.235275.

Molfese PJ, Glen D, Mesite L, Cox RW, Hoeft F, Frost SJ, Mencl WE, Pugh KR, Bandettini PA: **The Haskins Pediatric Atlas: An MRI-Based Pediatric Template and Atlas**. *Pediatr Radiol* [in press].

Finn ES, Huber L, Bandettini PA: **Higher and deeper: Bringing layer fMRI to association cortex**. *Prog Neurobiol*, 2020, doi.org/10.1016/j.pneurobio.2020.101930

Handwerker DA, Ianni G, Gutierrez B, Roopchansingh V, O'Connell K, Balderston N, Chen G, Bandettini PA, Ungerleider LG, Pitcher D, **Theta-burst TMS to the posterior superior temporal sulcus decreases resting-state fMRI connectivity across the face processing network,** Network Neuroscience, 1-15, 2019.

Bandettini PA, Huber L, Finn ES: **The Promise and Challenge of Layer Functional MRI for Deep Imaging**. *Curr Opin Behav Sci* [in press].

Book Chapter:

P. A. Bandettini and Hanzhang Lu, Magnetic Resonance Methodologies, Neurobiology of Mental Illness (Eric Nestler, Dennis Charney, Eds.) 2017.

Book:

fMRI, Peter Bandettini, MIT Press Essential Knowledge Series, Cambridge, 2020.

Non-SFIM papers co-authored by SFIM members since last BSC report (21 papers)

J Gonzalez-Castillo, R Michal, R. Monenam. "Towards expanded utility of realtime fMRI neurofeedback in clinical applications". Frontiers in Human Neuroscience, 14:471 (2020).

R Rolinski, X You, **J Gonzalez-Castillo**, G Norato, RC Reynolds, SK Inati, William H Theodore "Language lateralization from task-based and resting state functional MRI in patients with epilepsy" Human Brain Mapping, 41(11):3133-3146 (2020)

M Ramot, **J Gonzalez-Castillo**. "A framework for offline evaluation and optimization of real-time algorithms for use in neurofeedback, demonstrated on an instantaneous proxy for correlations" NeuroImage 188, 322-334 (2019)

S Torrisi, AX Gorka, **J Gonzalez-Castillo**, K O'Connell, N Balderston, Christian Grillon, Monique Ernst "Extended amygdala connectivity changes during sustained shock anticipation" Translational Psychiatry 8 (1), 33 (2018)

M Ramot, S Kimmich, **J Gonzalez-Castillo**, V Roopchansingh, H Popal, Emily White, Stephen J Gotts, Alex Martin "Direct Modulation of Aberrant Brain Network Connectivity Through Real-Time NeuroFeedback" eLife, e28974 (2017)

Luthra, S., Fuhrmeister, P., **Molfese, P.J.**, Guediche, S., Blumstein, S.E., & Myers, E.B. (2019). Brain-behavior relationships in incidental learning of non-native phonetic categories. Brain & Language, 198, 104692.

Hung, Y., Frost, S. J., **Molfese, P.**, Malins, J. G., Landi, N., Mencl, W. E., Rueckl, J. G., Bogaerts, L., Pugh, K. R. (2019). Common neural basis of motor sequence learning and word recognition and its relation with individual differences in reading skill. Scientific Studies of Reading, 23, 89-100.

Johns, C. L., Jahn, A., A., Jones, H. R., Kush, D., **Molfese, P. J.**, Van Dyke, J. A., Magnuson, J. S., Tabor, W., Mencl, W. E., Shankweiler, D. P., & Braze, D. (2018). Individual differences in decoding skill, print exposure, and cortical structure in young adults. Language, Cognition, and Neuroscience, 33, 1275-1295.

Michaels, T., Ly, M., Wang, L., Chen, C., **Molfese, P.**, Burke, J. (2018). S53. Combined Resting State fMRI and EEG Investigation of Irritability. Biological Psychchiatry, 83, S367.

Malins, J. G., Pugh, K. R., Buis, B., Frost, S. J., Hoeft, F., Landi, N., Mencl, W. E., Kurian, A., Staples, R., **Molfese, P. J.**, Sevcik, R., Morris, R. (2018). Individual differences in reading skill are related to trial-by-trial neural activation variability in the reading network. Journal of Neuroscience, 38, 2981-2989.

Landi, N., Malins, J. G., Frost, S. J., Magnuson, J. S., **Molfese, P.**, Ryherd, K., Rueckl, J. G., Mencl, W. E., Pugh, K. R. (2018). Neural representations for newly learned words are modulated by overnight consolidation, reading skill, and age. Neuropsychologia, 111, 133-144.

Todd, K. L., Brighton, T., Norton, E. S., Schick, S., Elkins, W., Pletnikova, O., Fortinsky, R. H., Troncoso, J. C., **Molfese, P. J.**, Resnick, S. M., Conover, J. C. (2018). Ventricular and Periventricular Anomalies in the Aging and Cognitively Impaired Brain. Frontiers in Aging Neuroscience, 9, 445.

Del Tufo, S. N., Frost, S. J., Hoeft, F., Cutting, L. E., **Molfese, P. J.**, Mason, G. F., Rothman, D. L., Fulbright, R. K., & Pugh, K. R. (2018). Neurochemistry predicts convergence of written and spoken language: a proton magnetic resonance spectroscopy study of cross-modal language integration. Frontiers in Psychology, 9.

Jasinska, K. K., **Molfese, P. J.**, Kornilov, S. A., Mencl, W. E., Frost, S. J., Lee, M., Pugh, K. R., Grigorenko, E. L., & Landi, N. (2017). The BDNF Val66Met Polymorphism is Associated with Neuroanatomical Differences in the Pediatric Brain with Implications for Cognitive Development. Behavioral Brain Research, 328, 48-56.

Persichetti AS, Avery JA, **Huber L,** Merriam EP, Martin A. Layer-Specific Contributions to Imagined and Executed Hand Movements in Human Primary Motor Cortex. Curr Biol. 2020;30:1-5.

Huber, L., Uludag, K., and Möller, H.E. (2017). Non-BOLD contrast for laminar fMRI in humans: CBF, CBV, and CMRO2. Neuroimage, doi: 10.1016/j.neuroimage.2017.07

Waugh, J. L., Kuster, J. K., Makhlouf, M. L., **Levenstein, J. M.**, Multhaupt-Buell, T. J., Warfield, S. K., ... & Blood, A. J. (2019). A registration method for improving quantitative assessment in probabilistic diffusion tractography. *NeuroImage*, *189*, 288-306.

Blood, A. J., Kuster*, J. K., Waugh*, J. L., **Levenstein*, J. M.**, Multhaupt-Buell, T. J., Sudarsky, R. L., ... & Sharma, N. (2019). White matter changes in cervical dystonia relate to clinical effectiveness of botulinum toxin treatment. *Frontiers in Neurology*, *10*, 265. ** equal contributions*

Johnstone*, A., **Levenstein*, J. M.**, Hinson, E. L., & Stagg, C. J. (2018). Neurochemical changes underpinning the development of adjunct therapies in recovery after stroke: A role for GABA?. *Journal of Cerebral Blood Flow & Metabolism*, *38*(9), 1564-1583. ** equal contributions*

Varjačić, A., Mantini, D., **Levenstein, J.**, Slavkova, E. D., Demeyere, N., & Gillebert, C. R. (2018). The role of left insula in executive set-switching: Lesion evidence from an acute stroke cohort. *cortex*, *107*, 92-101.

Waugh, J. L., Kuster, J. K., **Levenstein, J. M.,** Makris, N., Multhaupt-Buell, T. J., Sudarsky, L. R., ... & Blood, A. J. (2016). Thalamic volume is reduced in cervical and laryngeal dystonias. *PLoS One*, *11*(5), e0155302

Resource Sharing and Data Sharing

Datasets shared:

100 run study: 9 hours of scanning per subject for three subjects performing a simple motor-visual task.
Multi-task dataset: multiple 24-minute data sets consisting of 8 x 3-minute segments of four tasks: video, working memory, calculation, and rest.

We plan to deposit all our data into our NIH data repository that will be started through the Data Sharing Core Facility, headed by Adam Thomas. Until then, we will keep it in our own archives (NIH Biowulf Cluster) and will make available on request. De-identified data can be shared with any researcher who signs a data use agreement as defined in NIH IRB protocol 93M0170. Data has been shared through he central.xnat.org repository and using https://nihcesaev.cit.nih.gov for specific requests from non-NIH researchers.

We have shared example data upon request from:
Olivia Viessmann, James Kolasisnki, FMRIB, Oxford
Rosa Panchuelo and Susan Francis, Nottingham
Gopi (Kaundiniya Gopinath) from Emory University in Atlanta
Markus Barth from Queensland
Olivier Reynaud from Lausanne

Much of our code is made available through public GitHub repositories. We recently hired a scientific programmer, Jushua Teves, to help us both share and centralize our publicly shared code at https://github.com/nimh-sfim.

Collaborations

Alex Martin, NIMH LBC
Visual naming in simultaneous EEG+fMRI, and high resolution fMRI
Eli Merriam, NIMH LBC
High resolution fMRI
Chris Baker NIMH, LBC
High resolution fMRI
Leslie Ungerleider, NIMH, LBC
Co-author on TMS+fMRI project with Dan Handwerker
Bob Cox, Gang Chen, Dan Glen, NIMH, SSCC
help with AFNI
Sean Marrett, Vinai Roopchansingh, Andy Derbyshire, Linqing Li, NIMH, Functional MRI Core Facility
Help with scanning infrastructure, pulse sequences, data transfer and archival pipeline, subject interface
Francisco Pereira, NIMH, Machine Learning Team
Collaboration on machine learning-relevant analyses
Adam Thomas, NIMH, Data Science and Sharing Team
Help with sharing, management and analysis of public data sets
Benedikt Poser, University of Maastricht
He provided pulse sequence input regarding high resolution fMRI.
Carlos ZarateNIMH SSCC
collaborator on Emily Finn's K99 depression project
Christian Grillon NIMH
Co-author on multi-echo fMRI study of development
Elizabeth Hillman, Columbia University
We are on a grant together to investigate the relationship between Calcium Imaging Signals and fMRI signals.
Emily Meyers, University of Connecticut
Non-native speech sound learning impacted by sleep with fMRI/ISC
Jeff Duyn, NINDS,
Collaborating on MT contrast study for white matter delineation, and sleep studies
Lars Muckli, University of Glasgow
Provided visual/auditory motion paradigm for a layer activation experiment
Manish Saggar, Stanford University
Worked with us on our time series decoding project. We provided input for a paper that he published.
Michael Millham, Child Mind Institute
Provided data (from his database) for one of our naturalistic stimuli projects.
Sara Inati, NINDS,
Epilepsy and simultaneous EEG+fMRI
Sayako Earl, University of Delaware
Learning and sleep consolidation
Sunandra Mitra, University of Texas, Lubbock
Co-mentored a student we hosted in our lab. She co-authored several papers that he wrote while in our lab.
Todd Constable, Yale University
Provided some of the data regarding our naturalistic stimuli and cross subject correlation project.
Tristan Bekinchtein, Cambridge University
Co-mentor to graduate student Samika Kumar
Charlotte Stagg, Oxford University
Co-mentor to graduate student Jacob Levenstein
Vince Calhoun, Georgia Tech
Co-mentored a student we hosted in our lab. He was co-author on several of his papers that he wrote with us.

Angela Lard and Taylor Salo, Florida International University
Collaborator on multi-echo pipeline creation project: tedana.
Cesar Caballero-Gaudes, Basque Center of Cognition, San Sebastian, Spain
Co-authored several papers with us on deconvolution of fMRI using multi-echo data.
Eneko Uruñuela and Stephano Moia Basque Center of Cognition, San Sebastian, Spain
Collaborator on multi-echo pipeline project: tedana
Logan Dowdle, University of Minnesota,
Collaborator on multi-echo pipeline project: tedana
Kirstie Whitaker, Alan Turing Institute, London
Collaborator on multi-echo pipeline project: tedana
Julia Kam, University of Calgary, Alberta, CA
Co-authoring a paper in preparation on imaging ongoing thought. Collaborator on real time fMRI project.
Colin Hoy, University of California, Berkeley
Co-authoring a paper in preparation on imaging ongoing thought. Collaborator on real time fMRI project.
Peter Jezzard, Oxford University
Co-author on paper describing DANTE prepared dual-echo fMRI for while brain CBV quantification.
Tom Nichols, Oxford University
Co-author on paper assessing noise sources across trials, runs, and sessions.
Naryanan Srinivassan and Ishan Singhal, Indian Institute of Technology, Kanpur
Collaborated on our study of flip angle and its effects on resting-state connectivity.
Lilianne Mujica-Parodi, Stony Brook University School of Medicine
We are testing a dynamic phantom that she has provided us as we are collaborators on her grant supporting this.
Maria Acosta, National Human Genome Research Institute, NIH.
Advising with acquisition, analysis and interpretation of resting-state fMRI data in a gene therapy protocol looking at clinical outcomes of a novel Intravenous Gene Transfer with an AAV9 Vector Expressing Human β-galactosidase in Type II GM1 Gangliosidosis.

Resources Requested

2 additional post bac IRTA positions. We currently have 4 post bac IRTAs but two are here on temporary loan and will disappear once the loan ends. We feel that 4 post bac IRTA positions is optimal for us as we have 2 staff scientists and 2 post docs, and will shortly have 2 more post docs. We feel that the ratio of 2 post bac IRTAs for every 3 post docs is optimal.

Bibliography

1. Katwal SB, Gore JC, Gatenby JC, Rogers BP. Measuring relative timings of brain activities using fMRI. *Neuroimage*. 2013;66:436-448. doi:10.1016/j.neuroimage.2012.10.052
2. Menon* † ‡ § RS, Luknowsky DC, Gati JS. *Mental Chronometry Using Latency-Resolved Functional MRI*. Vol 95.; 1998. Accessed November 30, 2020. www.pnas.org.
3. Norris DG, Polimeni JR. Laminar (f)MRI: A short history and future prospects. *Neuroimage*. 2019;197:643-649. doi:10.1016/j.neuroimage.2019.04.082
4. Chai Y, Li L, Huber L, Poser BA, Bandettini PA. Integrated VASO and perfusion contrast: A new tool for laminar functional MRI. *Neuroimage*. 2020;207:116358. doi:10.1016/j.neuroimage.2019.116358
5. Huber L, Ivanov D, Handwerker DA, et al. Techniques for blood volume fMRI with VASO: From low-resolution mapping towards sub-millimeter layer-dependent applications. *Neuroimage*. 2018;164:131-143. doi:10.1016/j.neuroimage.2016.11.039
6. Huber L (Renzo) R (Renzo), Poser BA, Bandettini PA, et al. LAYNII: A software suite for layer-fMRI. *BioRxiv*. Published online June 14, 2020:2020.06.12.148080. doi:10.1101/2020.06.12.148080
7. Huber L, Finn ES, Chai Y, et al. Layer-dependent functional connectivity methods. *Prog Neurobiol*. Published online June 5, 2020:101835. doi:10.1016/j.pneurobio.2020.101835
8. Lu H, Golay X, Pekar JJ, Van Zijl PCM. Functional magnetic resonance imaging based on changes in vascular space occupancy. *Magn Reson Med*. 2003;50(2):263-274. doi:10.1002/mrm.10519
9. Huber L, Handwerker DA, Jangraw DC, et al. High-Resolution CBV-fMRI Allows Mapping of Laminar Activity and Connectivity of Cortical Input and Output in Human M1. *Neuron*. 2017;96(6):1253-1263.e7. doi:10.1016/j.neuron.2017.11.005
10. Huber L, Finn ES, Handwerker DA, et al. Sub-millimeter fMRI reveals multiple topographical digit representations that form action maps in human motor cortex. *Neuroimage*. 2020;208:116463. doi:10.1016/j.neuroimage.2019.116463
11. Leo A, Handjaras G, Bianchi M, et al. A synergy-based hand control is encoded in human motor cortical areas. *Elife*. 2016;5(FEBRUARY2016). doi:10.7554/eLife.13420
12. Yu Y, Huber L, Yang J, et al. Layer-specific activation of sensory input and predictive feedback in the human primary somatosensory cortex. *Sci Adv*. 2019;5(5):eaav9053. doi:10.1126/sciadv.aav9053
13. Finn ES, Huber L, Jangraw DC, Molfese PJ, Bandettini PA. Layer-dependent activity in human prefrontal cortex during working memory. *Nat Neurosci*. 2019;22(10):1687-1695. doi:10.1038/s41593-019-0487-z
14. Felleman DJ, Van Essen DC. Distributed hierarchical processing in the primate cerebral cortex. *Cereb Cortex*. 1991;1(1):1-47. doi:10.1093/cercor/1.1.1
15. Kazan SM, Huber L, Flandin G, Ivanov D, Bandettini P, Weiskopf N. Physiological basis of vascular autocalibration (VasA): Comparison to hypercapnia calibration methods. *Magn Reson Med*. 2017;78(3):1168-1173. doi:10.1002/mrm.26494
16. Li L, Miller KL, Jezzard P. DANTE-prepared pulse trains: A novel approach to motion-sensitized and motion-suppressed quantitative magnetic resonance imaging. *Magn Reson Med*. 2012;68(5):1423-1438. doi:10.1002/mrm.24142
17. Wu WC, Buxton RB, Wong EC. Vascular space occupancy weighted imaging with control of residual blood signal and higher contrast-to-noise ratio. *IEEE Trans Med Imaging*. 2007;26(10):1319-1327. doi:10.1109/TMI.2007.898554
18. Ciris PA, Qiu M, Constable RT. Noninvasive MRI measurement of the absolute cerebral blood volume-cerebral blood flow relationship during visual stimulation in healthy humans. *Magn Reson Med*. 2014;72(3):864-875. doi:10.1002/mrm.24984
19. Lu H, van Zijl PCM, Hendrikse J, Golay X. Multiple acquisitions with global inversion cycling (MAGIC): A multislice technique for vascular-space-occupancy dependent fMRI. *Magn Reson Med*. 2004;51(1):9-15. doi:10.1002/mrm.10659
20. Gonzalez-Castillo J, Hoy CW, Handwerker DA, et al. Tracking ongoing cognition in individuals using

brief, whole-brain functional connectivity patterns. *Proc Natl Acad Sci*. 2015;112(28):8762-8767. doi:10.1073/pnas.1501242112
21. Gonzalez-Castillo J, Caballero-Gaudes C, Topolski N, Handwerker DA, Pereira F, Bandettini PA. Imaging the spontaneous flow of thought: Distinct periods of cognition contribute to dynamic functional connectivity during rest. *Neuroimage*. 2019;202. doi:10.1016/j.neuroimage.2019.116129
22. Caballero Gaudes C, Petridou N, Francis ST, Dryden IL, Gowland PA. Paradigm free mapping with sparse regression automatically detects single-trial functional magnetic resonance imaging blood oxygenation level dependent responses. *Hum Brain Mapp*. 2013;34(3):501-518. doi:10.1002/hbm.21452
23. Hasson U, Nir Y, Levy I, Fuhrmann G, Malach R. Intersubject Synchronization of Cortical Activity during Natural Vision. *Science (80-)*. 2004;303(5664):1634-1640. doi:10.1126/science.1089506
24. Finn ES, Glerean E, Khojandi AY, et al. Idiosynchrony: From shared responses to individual differences during naturalistic neuroimaging. *Neuroimage*. 2020;215:116828. doi:10.1016/j.neuroimage.2020.116828
25. Finn ES, Bandettini PA. Movie-watching outperforms rest for functional connectivity-based prediction of behavior. *bioRxiv*. Published online 2020:2020.08.23.263723. doi:10.1101/2020.08.23.263723
26. Finn ES, Corlett PR, Chen G, Bandettini PA, Constable RT. Trait paranoia shapes inter-subject synchrony in brain activity during an ambiguous social narrative. *Nat Commun*. 2018;9(1):1-13. doi:10.1038/s41467-018-04387-2
27. Jangraw DC, Gonzalez-Castillo J, Handwerker DA, et al. A functional connectivity-based neuromarker of sustained attention generalizes to predict recall in a reading task. *Neuroimage*. 2018;166:99-109. doi:10.1016/j.neuroimage.2017.10.019
28. Chang C, Metzger CD, Glover GH, Duyn JH, Heinze H-J, Walter M. Association between heart rate variability and fluctuations in resting-state functional connectivity. *Neuroimage*. 2013;68:93-104. doi:10.1016/j.neuroimage.2012.11.038
29. Fultz NE, Bonmassar G, Setsompop K, et al. Coupled electrophysiological, hemodynamic, and cerebrospinal fluid oscillations in human sleep. *Science (80-)*. Published online 2019. doi:10.1126/science.aax5440
30. Yousefi B, Shin J, Schumacher EH, Keilholz SD. Quasi-periodic patterns of intrinsic brain activity in individuals and their relationship to global signal. *Neuroimage*. 2018;167:297-308. doi:10.1016/j.neuroimage.2017.11.043